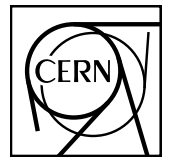


EUROPEAN ORGANIZATION FOR NUCLEAR RESEARCH



ALICE-ANA-2022-xxx
November 10, 2022

D^{*+}-meson production in pp collisions at $\sqrt{s} = 13$ TeV

Syaefudin Jaelani¹

1. Indonesian Institute of Sciences

Email: syaefudin.jaelani@cern.ch

Abstract

The production of prompt D^{*+} in pp collisions at $\sqrt{s} = 13$ TeV at the LHC are reported in this analysis note using the full pp data sample collected in 2016, 2017, and 2018. The production cross-section is measured at mid-rapidity as a function of p_T . The D^{*+} mesons were reconstructed using the decay channel D^{*+} → D⁰ π⁺, exploiting the D⁰ decay D⁰ → K⁻ π⁺. The D^{*+} mesons are reconstructed in the range $1 < p_T < 50$ GeV/ c . The p_T -differential cross sections are compared with QCD calculations.

Contents

1	Introduction	3
1.1	Data sample	3
1.2	Monte Carlo sample	7
1.3	Code used for the analysis	7
2	D^{*+}-meson selection	8
2.1	Single track selections	8
2.2	Topological and kinematic selections	8
2.3	Particle identification	8
2.4	Signal extraction	9
3	Corrections	9
4	Systematic uncertainties	13
4.1	Raw yield extraction	13
4.2	Selection efficiency	24
4.3	Generated p_T shape	26
4.4	PID efficiency	28
4.5	Track reconstruction efficiency	30
5	Feed-down subtraction	32
6	D^{*+}-meson systematics summary	33
7	Results	34

1 Introduction

1.1 Data sample

The analyses note will discuss the production cross-section of D^{*+}-meson in pp collisions at $\sqrt{s} = 13$ TeV. The data samples used for this analysis are pp data at $\sqrt{s} = 13$ TeV combined collected in 2016, 2017, and 2018. The minimum bias triggered data of data samples, LHC2016_deghjop, LHC2016_kl, LHC2017_cefhijklmor, and LHC2018_bdefghijklmnop are used for this analysis. The run numbers were used in the analysis, as selected after quality assurance, are reported below:

– LHC2016_AOD234_deghjop_13TeV

child 1: 252375, 252374, 252371, 252370, 252368, 252336, 252332, 252330, 252326, 252325, 252322, 252319, 252317, 252310, 252271, 252248, 252235
child 2: 253591, 253589, 253563, 253530, 253529, 253517, 253488, 253482, 253481, 253478, 253437, 252867, 252858
child 3: 254332, 254331, 254330, 254304, 254303, 254302, 254293, 254205, 254204, 254199, 254193, 254178, 254175, 254174, 254149, 254147, 254128
child 4: 255469, 255467, 255466, 255465, 255463, 255447, 255442, 255440, 255421, 255420, 255419, 255418, 255415, 255407, 255402, 255398, 255352, 255351, 255350, 255283, 255280, 255276, 255275, 255256, 255255, 255253, 255252, 255251, 255249, 255248, 255247, 255242, 255240, 255182, 255181, 255180, 255177, 255176, 255174, 255173, 255171, 255167, 255162, 255159, 255154, 255111, 255091, 255086, 255085, 255082, 255079, 254984, 254983, 254654, 254653, 254652, 254651, 254649, 254648, 254646, 254644, 254640, 254632, 254630, 254629, 254621, 254606, 254604, 254422, 254419, 254418
child 5: 256418, 256417, 256415, 256373, 256372, 256371, 256368, 256366, 256365, 256364, 256363, 256362, 256361, 256356, 256311, 256309, 256307, 256302, 256299, 256297, 256295, 256292, 256290, 256289, 256287, 256284, 256283, 256282, 256281, 256231, 256228, 256227, 256225, 256223, 256219
child 6: 264035, 264033, 263985, 263984, 263981, 263978, 263977, 263923, 263920, 263917, 263916, 263905, 263866, 263863, 263810, 263803, 263793, 263792, 263790, 263787, 263786, 263785, 263784, 263744, 263743, 263741, 263739, 263738, 263737, 263691, 263690, 263682, 263663, 263662, 263657, 263654, 263652, 263647, 263529, 263497, 263496, 263490, 263487, 263332, 263331, 262858, 262855, 262853, 262849, 262847, 262844, 262842, 262841, 262778, 262777, 262776, 262768, 262760, 262727, 262725, 262723, 262719, 262717, 262713, 262708, 262706, 262705, 262428, 262426, 262425, 262424, 263979, 262635, 262632, 262628, 262624, 262594, 262593, 262583, 262578, 262574, 262572, 262571, 262570, 262569, 262568, 262567, 262563, 262537, 262533, 262532, 262528, 262492, 262490, 262489, 262487, 262451, 262450, 262430, 263861
child 7: 264347, 264346, 264345, 264341, 264336, 264312, 264306, 264305, 264281, 264279, 264277, 264273, 264267, 264266, 264265, 264264, 264262, 264261, 264260, 264259, 264238, 264235, 264233, 264232, 264198, 264197, 264194, 264190, 264188, 264168, 264164, 264139, 264138, 264137, 264129, 264110, 264109, 264086, 264085, 264082, 264078, 264076

– LHC2016_AOD234_kl_13TeV

child 1: 258537, 258499, 258477, 258456, 258454, 258452, 258426, 258393, 258391, 258387, 258359, 258336, 258332, 258307, 258306, 258303, 258302, 258301, 258299, 258278, 258274, 258273, 258271, 258270, 258258, 258257, 258256, 258204, 258203, 258202, 258198, 258197, 258178, 258117, 258114, 258113, 258109, 258108, 258107, 258063, 258062, 258060, 258059, 258053, 258049, 258045, 258042, 258041, 258039, 258019, 258017, 258014, 258012, 258008, 258003, 257992, 257989, 257986, 257979, 257963, 257960, 257957, 257939, 257937, 257936,

257855, 257853, 257851, 257850, 257804, 257803, 257800, 257799, 257798, 257797, 257773, 257765, 257757, 257754, 257737, 257735, 257734, 257733, 257727, 257725, 257724, 257697, 257694, 257692, 257691, 257689, 257688, 257687, 257685, 257684, 257682, 257644, 257642, 257636, 257635, 257632, 257630, 257606, 257605, 257604, 257601, 257595, 257594, 257592, 257590, 257588, 257587, 257566, 257562, 257561, 257560, 257541, 257540, 257539, 257537, 257531, 257530, 257492, 257491, 257490, 257488, 257487, 257474, 257468, 257457, 257433, 257364, 257358, 257330, 257322, 257320, 257318, 257260, 257224, 257209, 257206, 257204, 257144, 257141, 257139, 257138, 257137, 257136, 257100, 257095, 257092, 257086, 257084, 257082, 257080, 257077, 257012, 257011, 256944, 256942, 256941, 258498, 258388, 258280, 257932, 257912, 257901, 257071

child 2: 259888, 259868, 259867, 259866, 259860, 259842, 259841, 259822, 259789, 259788, 259781, 259756, 259752, 259751, 259750, 259748, 259747, 259477, 259473, 259396, 259395, 259394, 259389, 259388, 259382, 259378, 259342, 259341, 259340, 259339, 259336, 259334, 259307, 259305, 259303, 259302, 259274, 259273, 259272, 259271, 259270, 259269, 259264, 259263, 259261, 259257, 259204, 259164, 259162, 259118, 259117, 259099, 259096, 259091, 259090, 259088, 258964, 258962, 259381, 259086

- LHC2017_AOD234_cefhijklmor_13TeV_pp

child 1: 270830, 270828, 270827, 270824, 270822

child 2: 270865, 270861, 270856, 270855, 270854

child 3: 273103, 273100, 273099, 273077, 273010, 273009, 272985, 272983, 272976, 272949, 272947, 272939, 272935, 272934, 272933, 272932, 272905, 272903, 272880, 272873, 272871, 272870, 272836, 272834, 272833, 272829, 272828, 272784, 272783, 272782, 272764, 272763, 272760, 272749, 272747, 272712, 272691, 272690, 272620, 272610, 272608, 272607, 272585, 272577, 272575, 272574, 272521, 272468, 272466, 272463, 272462, 272461, 272413, 272411, 272400, 272399, 272395, 272394, 272389, 272388, 272360, 272359, 272340, 272335, 272194, 272156, 272155, 272154, 272153, 272152, 272151, 272123, 272101, 272100, 272076, 272042, 272040, 272039, 272038, 272036, 272020, 272018, 271886, 271880, 271874, 271873, 271871, 271870, 273101, 272762, 272469, 272417, 272414, 272075

child 4: 274442, 274390, 274389, 274388, 274387, 274386, 274385, 274364, 274363, 274360, 274352, 274329, 274283, 274281, 274280, 274278, 274276, 274271, 274270, 274269, 274268, 274266, 274264, 274263, 274259, 274258, 274232, 274212, 274174, 274148, 274147, 274125, 274094, 274092, 274058, 273986, 273985, 273946, 273943, 273942, 273918, 273889, 273887, 273886, 273885, 273825, 273824, 273654, 273653, 273593, 273592, 273591, 274357, 274355, 274063

child 5: 274671, 274669, 274667, 274657, 274653, 274601, 274596, 274595, 274594, 274593

child 6: 276508, 276507, 276506, 276462, 276439, 276438, 276437, 276435, 276351, 276348, 276302, 276297, 276294, 276292, 276290, 276259, 276257, 276230, 276205, 276178, 276177, 276170, 276169, 276166, 276145, 276140, 276135, 276104, 276102, 276099, 276098, 276097, 275847, 275664, 275661, 275650, 275648, 275647, 275624, 275623, 275622, 275621, 275617, 275612, 275559, 275558, 275515, 275472, 275471, 275467, 275459, 275457, 275456, 275453, 275452, 275448, 275443, 275406, 275404, 275401, 275372, 275369, 275361, 275360, 275333, 275332, 275328, 275326, 275324, 275322, 275314, 275283, 275247, 275246, 275245, 275239, 275188, 275184, 275180, 275177, 275174, 275173, 275151, 275150, 275149, 275076, 275075, 275073, 275068, 275067, 274979, 274978, 274886, 274882, 274878, 274877, 274822, 274821, 274815, 274806, 274803, 274802, 274801, 274708, 274690, 274736, 274883, 274884, 274889, 276105, 276108, 276141

child 7: 278216, 278215, 278191, 278189, 278167, 278166, 278165, 278164, 278158, 278127, 278126, 278123, 278122, 278121, 277996, 277991, 277989, 277987, 277952, 277930, 277907, 277904, 277903, 277900, 277899, 277898, 277897, 277876, 277870, 277848, 277847, 277845,

277842, 277841, 277836, 277834, 277805, 277802, 277801, 277800, 277799, 277795, 277794, 277749, 277747, 277746, 277745, 277725, 277723, 277722, 277721, 277577, 277576, 277575, 277574, 277537, 277536, 277534, 277531, 277530, 277479, 277478, 277477, 277476, 277473, 277472, 277418, 277417, 277416, 277389, 277386, 277385, 277384, 277383, 277360, 277314, 277312, 277310, 277293, 277262, 277257, 277256, 277197, 277196, 277194, 277193, 277189, 277188, 277184, 277183, 277182, 277181, 277180, 277155, 277121, 277117, 277091, 277087, 277082, 277079, 277076, 277073, 277037, 277017, 277016, 277015, 276972, 276971, 276970, 276969, 276967, 276920, 276917, 276916, 276762, 276675, 276674, 276672, 276671, 276670, 276644, 276608, 276557, 276556, 276553, 276552, 276551, 278130, 277988, 277470, 276669
child 8: 280140, 280135, 280134, 280131, 280126, 280118, 280114, 280111, 280108, 280107, 280066, 280052, 280051, 279879, 279855, 279854, 279853, 279830, 279827, 279826, 279773, 279749, 279747, 279719, 279718, 279715, 279689, 279688, 279687, 279684, 279683, 279682, 279679, 279677, 279676, 279642, 279641, 279632, 279630, 279559, 279550, 279491, 279488, 279487, 279483, 279441, 279439, 279435, 279410, 279391, 279355, 279354, 279349, 279348, 279344, 279342, 279312, 279310, 279309, 279274, 279273, 279270, 279268, 279267, 279265, 279264, 279242, 279238, 279235, 279234, 279232, 279208, 279207, 279201, 279199, 279157, 279155, 279130, 279123, 279122, 279118, 279117, 279107, 279106, 279075, 279074, 279073, 279069, 279068, 279044, 279043, 279041, 279036, 279035, 279008, 279007, 279005, 279000, 278999, 278964, 278963, 278960, 278959, 278941, 278939, 278936, 278915, 278914
child 9: 282704, 282703, 282702, 282700, 282677, 282676, 282673, 282671, 282670, 282667, 282666, 282651, 282629, 282622, 282620, 282618, 282609, 282608, 282607, 282606, 282580, 282579, 282575, 282573, 282546, 282545, 282544, 282528
child 10: 280283, 280284, 280285, 280286, 280290, 280310, 280312, 280348, 280349, 280350, 280351, 280374, 280375, 280403, 280405, 280406, 281961, 281956, 281953, 281940, 281939, 281932, 281931, 281928, 281920, 281918, 281916, 281915, 281895, 281894, 281893, 281892, 281633, 281592, 281583, 281574, 281569, 281568, 281563, 281562, 281557, 281511, 281509, 281477, 281475, 281450, 281449, 281446, 281444, 281443, 281441, 281415, 281321, 281301, 281277, 281275, 281273, 281271, 281244, 281243, 281242, 281241, 281240, 281213, 281212, 281191, 281190, 281189, 281181, 281180, 281179, 281081, 281080, 281062, 281061, 281060, 281036, 281035, 281033, 281032, 280999, 280998, 280997, 280996, 280994, 280990, 280947, 280943, 280940, 280936, 280897, 280880, 280856, 280854, 280849, 280848, 280847, 280844, 280842, 280793, 280792, 280787, 280786, 280768, 280767, 280766, 280765, 280764, 280763, 280762, 280761, 280757, 280756, 280755, 280754, 280753, 280729, 280706, 280705, 280681, 280679, 280671, 280647, 280645, 280639, 280637, 280636, 280634, 280613, 280583, 280581, 280574, 280551, 280550, 280547, 280546, 280519, 280518, 280499, 280490, 280448, 280447, 280446, 280445, 280443, 280419, 280415, 280412, 281756, 281755, 281754, 281753, 281751, 281750, 281741, 281713, 281709, 281707, 281706, 281705, 281581, 281580, 280676, 280673, 280650, 280648, 280352

– LHC2018_AOD264_bdefghijklmnop_13TeV

child 1: 286350, 286349, 286348, 286345, 286341, 286340, 286337, 286336, 286314, 286313, 286312, 286311, 286310, 286309, 286308, 286289, 286288, 286287, 286284, 286282, 286263, 286261, 286258, 286257, 286254, 286231, 286230, 286229, 286203, 286202, 286201, 286199, 286198, 286159, 286130, 286129, 286127, 286124, 286064, 286025, 286027, 286014, 285980, 285979, 285978, 286028, 286030

child 2: 286937, 286936, 286933, 286932, 286931, 286930, 286911, 286910, 286907, 286877, 286876, 286874, 286852, 286850, 286846, 286809, 286805, 286801, 286799, 286731, 286695, 286661, 286653, 286633, 286592, 286591, 286569, 286568, 286567, 286566, 286511, 286509, 286508, 286502, 286482, 286455, 286454, 286428, 286427, 286426, 286380

child 3: 287658, 287657, 287656, 287654, 287578, 287575, 287524, 287521, 287518, 287517,

287516, 287513, 287486, 287484, 287481, 287480, 287451, 287413, 287389, 287388, 287387, 287385, 287381, 287380, 287360, 287356, 287355, 287353, 287349, 287347, 287346, 287344, 287343, 287325, 287324, 287323, 287283, 287254, 287251, 287250, 287249, 287248, 287209, 287208, 287204, 287203, 287202, 287201, 287185, 287155, 287137, 287077, 287072, 287071, 287066, 287064, 287063, 287021, 287000, 287977, 287975, 287941, 287923, 287915, 287913, 287912, 287911, 287885, 287884, 287877, 287876, 287784, 287783

child 4: 288619, 288640, 288642, 288644, 288650, 288687, 288689, 288690, 288743, 288748, 288750

child 5: 288804, 288806

child 6: 288861, 288862, 288863, 288864, 288868, 288902, 288903, 288908, 288909, 288897

child 7: 288943

child 8: 289165, 289166, 289167, 289169, 289172, 289175, 289176, 289177, 289198, 289199, 289200, 289201

child 9: 289971, 289966, 289965, 289943, 289941, 289940, 289935, 289931, 289928, 289884, 289880, 289879, 289857, 289856, 289855, 289854, 289852, 289849, 289830, 289818, 289817, 289816, 289815, 289814, 289811, 289808, 289775, 289757, 289732, 289731, 289729, 289724, 289723, 289721, 289666, 289664, 289660, 289659, 289658, 289657, 289634, 289632, 289625, 289582, 289577, 289576, 289574, 289547, 289521, 289494, 289493, 289468, 289466, 289465, 289463, 289462, 289444, 289426, 289374, 289373, 289370, 289369, 289368, 289367, 289366, 289365, 289356, 289355, 289354, 289353, 289309, 289308, 289306, 289303, 289300, 289281, 289280, 289278, 289277, 289276, 289275, 289254, 289253, 289249, 289247, 289243, 289242, 289241, 289240, 289666, 289664, 289660, 289659, 289658, 289657, 289634, 289632, 289625, 289582, 289577, 289576, 289574

child 10: 292839, 292836, 292834, 292832, 292831, 292811, 292810, 292809, 292804, 292803, 292752, 292750, 292748, 292747, 292744, 292739, 292737, 292704, 292701, 292698, 292696, 292695, 292693, 292586, 292584, 292563, 292560, 292559, 292557, 292554, 292553, 292526, 292524, 292523, 292521, 292500, 292497, 292496, 292495, 292461, 292460, 292457, 292456, 292434, 292432, 292430, 292429, 292428, 292406, 292405, 292398, 292397, 292298, 292273, 292265, 292242, 292241, 292240, 292218, 292192, 292168, 292167, 292166, 292164, 292163, 292162, 292161, 292160, 292140, 292115, 292114, 292109, 292108, 292107, 292106, 292081, 292080, 292077, 292075, 292067, 292062, 292061, 292060, 292040, 292012, 291982, 291977, 291976, 291953, 291948, 291946, 291945, 291944, 291943, 291942, 291803, 291796, 291795, 291769, 291768, 291766, 291762, 291760, 291756, 291755, 291729, 291706, 291698, 291697, 291690, 291665, 291661, 291657, 291626, 291624, 291622, 291618, 291615, 291614, 291590, 291485, 291484, 291482, 291481, 291457, 291456, 291453, 291451, 291447, 291424, 291420, 291417, 291416, 291402, 291400, 291399, 291397, 291377, 291375, 291373, 291363, 291362, 291361, 291360, 291286, 291285, 291284, 291282, 291266, 291265, 291263, 291262, 291257, 291240, 291209, 291188, 291143, 291116, 291111, 291110, 291101, 291100, 291093, 291069, 291066, 291065, 291041, 291037, 291035, 291006, 291005, 291004, 291003, 291002, 290980, 290979, 290976, 290975, 290974, 290948, 290944, 290943, 290941, 290935, 290932, 290895, 290894, 290888, 290887, 290886, 290862, 290860, 290853, 290848, 290846, 290843, 290841, 290790, 290787, 290766, 290689, 290687, 290665, 290660, 290645, 290632, 290627, 290615, 290614, 290613, 290612, 290590, 290588, 290553, 290550, 290549, 290544, 290540, 290539, 290538, 290501, 290500, 290499, 290469, 290467, 290459, 290458, 290456, 290427, 290426, 290425, 290423, 290412, 290411, 290404, 290401, 290399, 290376, 290375, 290374, 290350, 290327, 290323, 291373

child 11: 293357, 293359

child 12: 293898, 293896, 293893, 293891, 293886, 293856, 293831, 293830, 293829, 293809, 293807, 293806, 293805, 293802, 293776, 293774, 293773, 293770, 293741, 293740, 293698, 293696, 293695, 293692, 293691, 293588, 293587, 293583, 293582, 293579, 293578, 293573,

293571, 293570, 293475, 293496, 293494, 293474, 293424, 293413, 293392, 293386, 293368
child 13: 294925, 294916, 294884, 294883, 294880, 294875, 294852, 294818, 294817, 294816,
294815, 294813, 294809, 294805, 294775, 294774, 294772, 294769, 294749, 294747, 294746,
294745, 294744, 294742, 294741, 294722, 294718, 294715, 294710, 294703, 294653, 294636,
294633, 294632, 294593, 294591, 294590, 294587, 294586, 294563, 294562, 294558, 294556,
294553, 294531, 294530, 294529, 294527, 294526, 294525, 294524, 294310, 294308, 294307,
294305, 294242, 294241, 294212, 294210, 294208, 294205, 294201, 294200, 294199, 294156,
294155, 294154, 294152, 294131, 294013, 294012, 294011, 294010, 294009
child 14: 285396, 285365, 285364, 285347, 285328, 285327, 285224, 285222, 285203, 285202,
285200, 285165, 285127, 285125, 285108, 285106, 285066, 285065, 285064, 285015, 285014,
285013, 285012, 285011, 285009

1.2 Monte Carlo sample

The Monte-Carlo (MC) sample used for the corrections is anchored to the run numbers reported above and generated with the same detector configurations as the data productions. In particular three production cycles are used LHC20f4a_2018_P8, LHC20f4b_2017_P8, and LHC20f4c_2016_P8. The Monte Carlo sample are generated with HIJING + HF Pythia8 events. Each pp event was required to contain at least one charm or beauty quark-antiquark pair. The following heavy-flavour hadrons are forced to decay via their hadronic decay channels. The run numbers used for the MC are the same as stated above for LHC2016, LHC2017, and LHC2018 samples.

1.3 Code used for the analysis

The results reported in this analysis note obtained with code available on AliPhysics Git master branch and more precisely in PWGHF/vertexingHF. The D^{*+} invariant mass distributions are obtained by using the task `AliAnalysisTaskSEDStarSpectra.cxx`. It reads the AOD event and looks over the D^{*+} candidates stored in the delta AOD, `AliAOD.VertexingHF`, at the filtering time. Single track, topological selections as well as particle identification are applied by using the class `AliRDHFDstartoKpipi` and the actual values of the cuts are read from a cut object saved as root file. The cut object is created using the AliRoot macro named `makeTFileDstartoKpipi`. The `AliHFInvMassFitter` was used to fit invariant mass distributions and estimate raw yields.

The D^{*+}-meson cut objects is also provided to the `AliAnalysisTaskCFVertexingHF`, which is the task used for the efficiencies evaluation for the correction of the raw yields. The results presented in this note are obtained by using ALICE LEGO trains. The results reported here are extracted from the output of the D2H pp LEGO trains. In particular, the data train numbers 4371-4374 and MC train numbers 3855-3857 were used. The topological selections used for the analyses can be found later in this note and are even saved in the LEGO train output.

2 D^{*+}-meson selection

The D^{*+}-meson and their anti-particles was reconstructed in the central rapidity region by exploiting their charged hadronic decay channels: D^{*+} → D⁰ π⁺ (with B.R. = $67.7 \pm 0.5\%$), while the D⁰ meson decay into K⁻ and π⁺ with branching ratio ($3.93 \pm 0.04\%$). The D^{*+} decay proceeds via strong interaction, thus making impossible the secondary vertex reconstruction. The analysis exploits topological selections on the D⁰, together with the sharp peak in the difference between the invariant mass of the three final state hadrons and that of the two D⁰ decay prongs. Since the mass difference $\Delta M = M_{D^{*+}} - M_{D^0} \approx 145.4$ MeV/c is only slightly larger than the charged pion mass. For low p_T D^{*+} mesons the produced pion has typically low momentum and is referred to here as a soft pion.

2.1 Single track selections

The D^{*+} candidates were formed by combining D⁰ candidates with soft pion π⁺ tracks having $|\eta| < 0.8$ and $p_T > 0.3$ GeV/c, also satisfying the kITSrefit and kTPCrefit conditions. Moreover, for all the tracks, a minimum number of 70 crossed rows in the TPC together with a crossed rows over findable clusters ratio of 0.8 was required, and $\chi^2/ndf < 2$ in the TPC. A cut on the transverse impact parameter d_0 was applied for tracks with $p_T < 2$ GeV/c, requiring $d_0 > 50$ μm. These selections were meant to limit the CPU time needed to perform the track combinatorics when creating the AODs with the D meson candidates. Furthermore, the D^{*+} soft pions were selected requiring at least one associated hit in either of the two SPD layers.

2.2 Topological and kinematic selections

The D^{*+} signal extraction is based on topological selections of displaced secondary vertices from D⁰-meson candidates. For a detailed explanation of the procedure refer to [1]. The topological and kinematic cuts used to select the D^{*+}-meson signal in pp collisions at $\sqrt{s} = 13$ TeV are reported in Table 1 and 2.

Table 1: Selections used for the D^{*+}-meson in the transverse momentum intervals $1 < p_T < 6.5$ GeV/c.

p_T (GeV/c) variable	[1-1.5]	[1.5-2]	[2-2.5]	[2.5-3]	[3-3.5]	[3.5-4]	[4-4.5]	[4.5-5]	[5-5.5]	[5.5-6]	[6-6.5]
ΔM_{D^0} (GeV)	0.021	0.032	0.035	0.035	0.038	0.038	0.038	0.042	0.042	0.045	0.049
DCA (cm)	0.022	0.038	0.03	0.03	0.03	0.03	0.042	0.042	0.05	0.05	0.1
$\text{Cos}(\theta^*)$	0.9	0.9	0.8	0.8	0.8	0.8	0.9	0.9	1.0	1.0	1.0
$p_T(K)$ (GeV/c)	0.4	0.4	0.9	0.9	0.9	1.0	1.0	1.0	1.0	1.0	1.0
$p_T(\pi)$ (GeV/c)	0.4	0.4	0.9	0.9	0.9	1.0	1.0	1.0	1.0	1.0	1.0
$d_{0,K}$ (cm)	0.1	0.1	0.1	0.1	0.1	0.1	0.1	0.1	0.1	0.1	0.1
$d_{0,\pi}$ (cm)	0.1	0.1	0.1	0.1	0.1	0.1	0.1	0.1	0.1	0.1	0.1
$d_{0,K} \times d_{0,\pi} (10^{-3})$ (cm ²)	-0.00025	-0.00025	-0.00019	-0.00014	-0.000144	-0.000144	-2.8×10^{-5}	-2.8×10^{-5}	5.5×10^{-5}	5.5×10^{-5}	0.0001
$\text{Cos}(\theta_{point})$	0.8	0.8	0.9	0.9	0.89	0.89	0.81	0.81	0.79	0.79	0.7
Inv. mass half width of D ^{*+} (GeV)	0.3	0.3	0.3	0.3	0.3	0.3	0.3	0.3	0.3	0.3	0.3
hal width of ΔM (GeV)	0.3	0.3	0.3	0.3	0.3	0.3	0.3	0.3	0.3	0.3	0.3
p_T soft π min (GeV/c)	0.05	0.05	0.05	0.05	0.05	0.05	0.05	0.05	0.05	0.05	0.05
p_T soft π max (GeV/c)	0.3	0.3	0.4	0.4	0.6	0.6	0.6	100	100	100	100
θ	1.0	1.0	1.0	1.0	1.0	1.0	1.0	1.0	1.0	1.0	1.0
$ \text{Cos}(\theta_{point})XY $	0.88	0.88	-1.	-1.	-1.	-1.	-1.	-1.	-1.	-1.	-1.
NL _{XY}	3.	3.	3.	3.	0	0	0	0	0	0	0

2.3 Particle identification

The identification of the charged kaons and pions in the TPC and TOF detectors provide an additional information for the background rejection in the low momentum region. In order to assign K and/or π masses to the decay tracks, cuts are applied to the difference in the expected and measured signals, which are the specific energy deposited (dE/dx) in the TPC and the time-of-flight for the TOF. A 3σ compatibility was required to D^{*+} candidate's daughters. When tracks were without TOF signal, only the TPC particle identification was used. Tracks with contradicting particle identification were considered to be non-identified and retained for further analysis.

Table 2: Selections used for the D^{*+}-meson in the transverse momentum intervals $6.5 < p_T < 50$ GeV/c.

p_T (GeV/c) variable	[6.5-7]	[7-7.5]	[7.5-8]	[8-9]	[9-10]	[10-12]	[12-16]	[16-24]	[24-36]	[36-50]
ΔM_{D^0} (GeV)	0.049	0.052	0.052	0.056	0.056	0.074	0.074	0.074	0.074	0.074
DCA (cm)	0.1	0.1	0.1	0.1	0.1	0.1	0.1	0.1	10	10
$\text{Cos}(\theta^*)$	1.0	1.0	1.0	1.0	1.0	1.0	1.0	1.0	10	10
$p_T(K)$ (GeV/c)	1.0	0.6	0.6	0.6	0.6	0.6	0.6	0.5	0.2	0.2
$p_T(\pi)$ (GeV/c)	1.0	0.6	0.6	0.6	0.6	0.6	0.6	0.5	0.2	0.2
$d_{0,K}$ (cm)	0.1	0.1	0.1	0.1	0.1	0.1	0.1	0.15	0.5	0.5
$d_{0,\pi}$ (cm)	0.1	0.1	0.1	0.1	0.1	0.1	0.1	0.15	0.5	0.5
$d_{0,K} \times d_{0,\pi} (10^{-3})$ (cm ²)	0.0001	0.0001	0.00019	0.0001	0.0001	0.001	0.001	1.	1.	1.
$\text{Cos}(\theta_{point})$	0.7	0.7	0.7	0.7	0.7	0.7	0.7	0.2	0.2	0.2
Inv. mass half width of D ^{*+} (GeV)	0.3	0.3	0.3	0.3	0.3	0.3	0.3	0.3	0.3	0.3
hal width of ΔM (GeV)	0.3	0.3	0.3	0.3	0.3	0.3	0.3	0.3	0.3	0.3
p_T soft π min (GeV/c)	0.05	0.05	0.05	0.05	0.05	0.05	0.05	0.05	0.05	0.05
p_T soft π max (GeV/c)	100	100	100	100	100	100	100	100	100	100
θ	1.0	1.0	1.0	1.0	1.0	1.0	1.0	1.0	1.0	1.0
$ \text{Cos}(\theta_{point})XY $	-1.	-1.	-1.	-1.	-1.	-1.	-1.	-1.	-1.	-1.
NL _{XY}	0	0	0	0	0	0	0	0	0	0

2.4 Signal extraction

The D^{*+} raw yields were extracted by performing a fit to the mass difference $\Delta M = M(K\pi\pi) - M(K\pi)$ distributions and the term describing the background shape is an exponential convoluted with a power law according to the equation:

$$f_{bkg} = a \sqrt{\Delta M - m_\pi} \cdot e^{b(\Delta M - m_\pi)} \quad (1)$$

where m_π is the pion mass and a and b are free parameters.

The D^{*+} ΔM invariant mass distribution is shown in Figure 1. For the p_T range 1-1.5 GeV/c, the power function was used to described the background shape. Figures 3 and 4 show that for the first p_T bin $1 < p_T < 1.5$ GeV/c, the power function was better to describe the background shape than the function mentioned in Eq (1), power law \times exponential function. The D^{*+} signal was successfully extracted in the range $1 < p_T < 50$ GeV/c. The goodness of the mass fit against the Monte Carlo (MC) expectations was checked in terms of mass peak σ and position. The comparisons of the Gaussian width and mean of the D^{*+} meson mass peaks in data and MC are reported in figure 2.

3 Corrections

The raw yields extracted from the fits to the invariant-mass distributions of D-meson candidates were corrected to obtain the p_T -differential production cross sections of prompt (i.e. not coming from weak decays of B mesons) D mesons. For example, in the case of D^{*+} mesons, the production cross section was calculated as:

$$\frac{d\sigma^{D^{*+}}}{dp_T} \Big|_{|y|<0.5} = \frac{1}{\Delta p_T} \frac{1}{BR \cdot L_{int}} \frac{f_{\text{prompt}}(p_T) \cdot \frac{1}{2} N^{D^{*+}\text{raw}}(p_T)}{2y_{\text{fid}}(p_T)(\text{Acc} \times \varepsilon)_{\text{prompt}}(p_T)} \quad (2)$$

where $N^{D^{*+}\text{raw}}$ (p_T) are the values of the raw yields (sum of particles and antiparticles), which were corrected for the B-meson decay feed-down contribution (i.e. multiplied by the prompt fraction f_{prompt}), divided by the acceptance-times-efficiency for prompt D^{*+} mesons, $(\text{Acc} \times \varepsilon)_{\text{prompt}}$, and divided by a factor of two to obtain the charge (particle and antiparticle) averaged yields. The corrected yields were divided by the decay channel branching ratio (BR), the p_T interval width (Δp_T), the rapidity coverage ($2y_{\text{fid}}$) and the integrated luminosity L_{int} . The integrated luminosity as computed from the number of

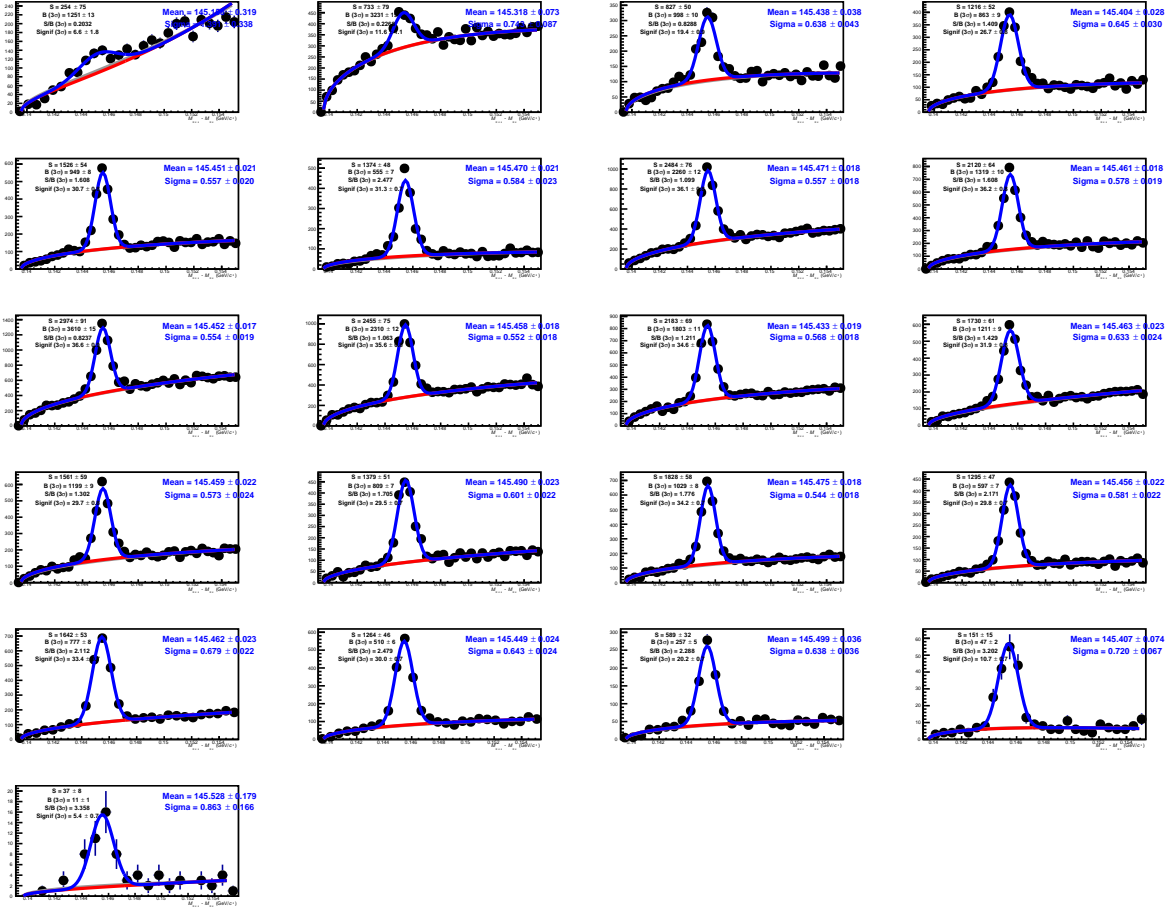


Fig. 1: The ΔM invariant mass distributions of D^{*+} candidates and charge conjugates in the p_T range $1 < p_T < 50$ GeV/c.

analyzed events and the cross section of pp collisions passing the minimum-bias trigger condition, σ_{pp} , MB = 57.95 mb, derived from a van der Meer scan measurement.

The acceptance and efficiency correction factors, $(\text{Acc} \times \epsilon)$, were determined using Monte Carlo simulations of pp collisions generated with the PYTHIA8 event generator with the Perugia-0 tune. The particles were propagated through the apparatus using both the GEANT transport codes. The luminous region distribution and the conditions (active channels, gain, noise level, and alignment) of all the ALICE detectors were included in the simulations, considering also their evolution with time during the LHC data taking period. The MC productions used to compute the $(\text{Acc} \times \epsilon)$ only events containing a $c\bar{c}$ or a $b\bar{b}$ pair were transported through the apparatus and reconstructed. Moreover, D mesons were forced to decay in the hadronic channels considered in this analysis. The efficiency was extracted separately for prompt D^{*+} and D^{*+} coming from B-meson decays (feed-down). The results are reported in figure 5.

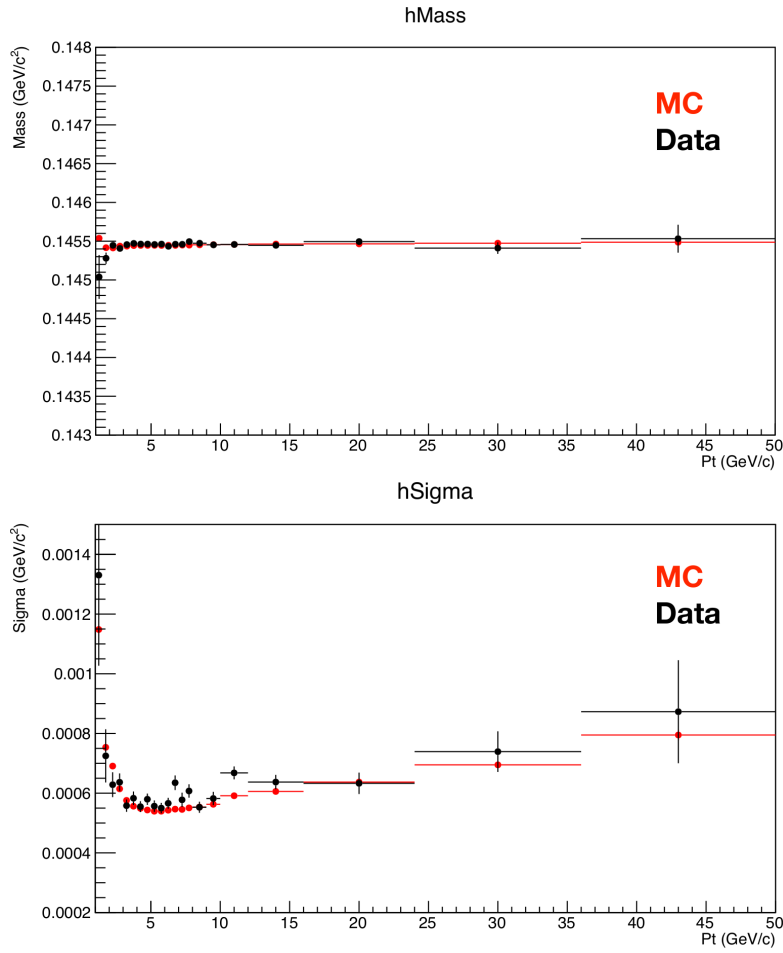


Fig. 2: Comparison of Gaussian mean (top) and width (bottom) extracted from the invariant-mass fits of D^{*+} candidates (black) and the MC simulation (red).

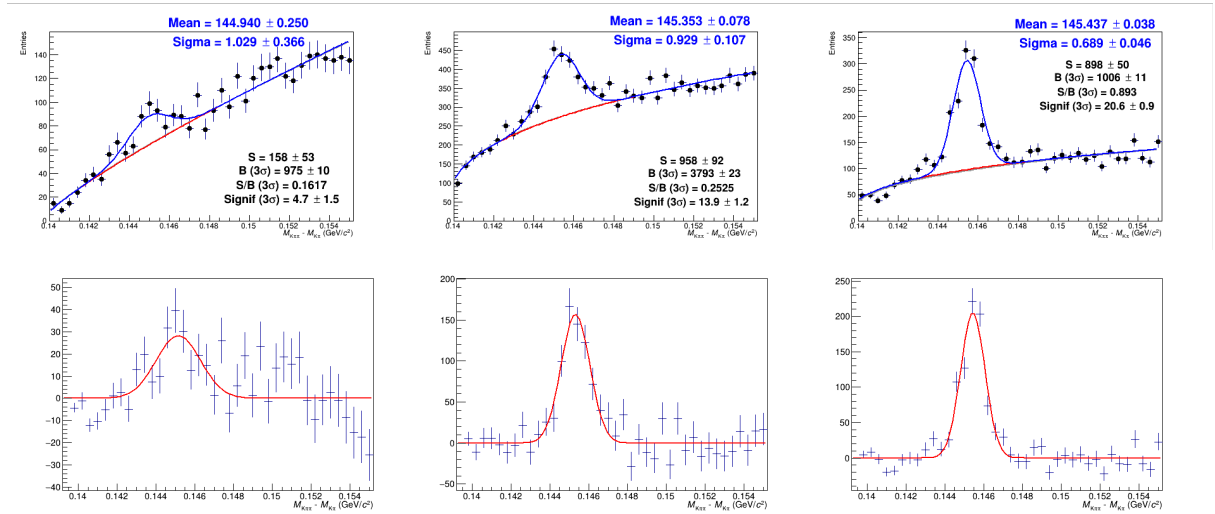


Fig. 3: The D^{*+} ΔM invariant mass distribution for p_T range 1-2.5 GeV/c (top rows) with the Power \times Exponential function for describing the background shape and the residual plots (bottom rows).

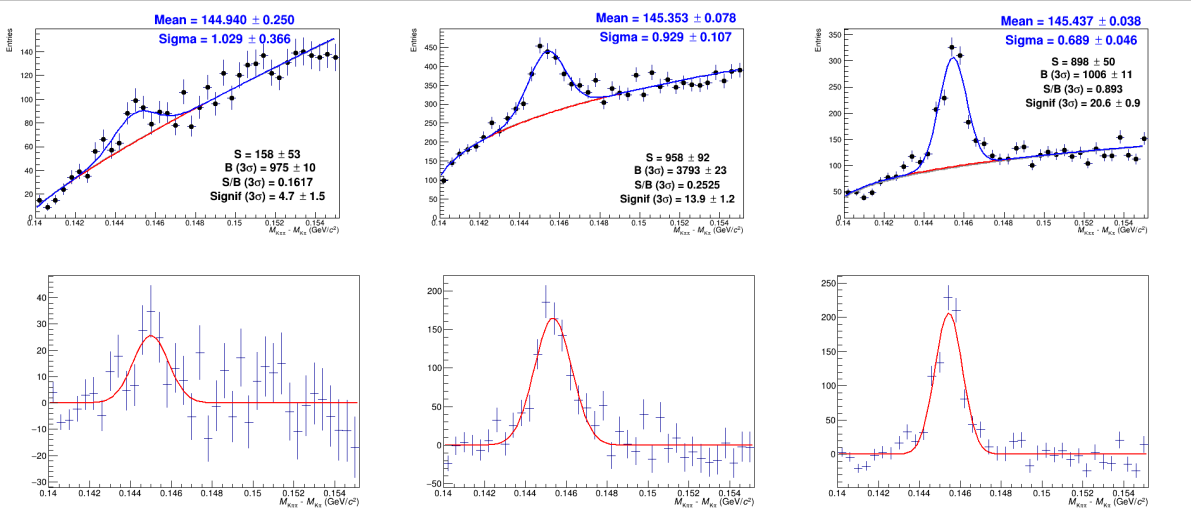


Fig. 4: The $D^{*+} \Delta M$ invariant mass distribution for p_T range 1-2.5 GeV/c (top rows) with the Power Law function for describing the background shape and the residual plots (bottom rows).

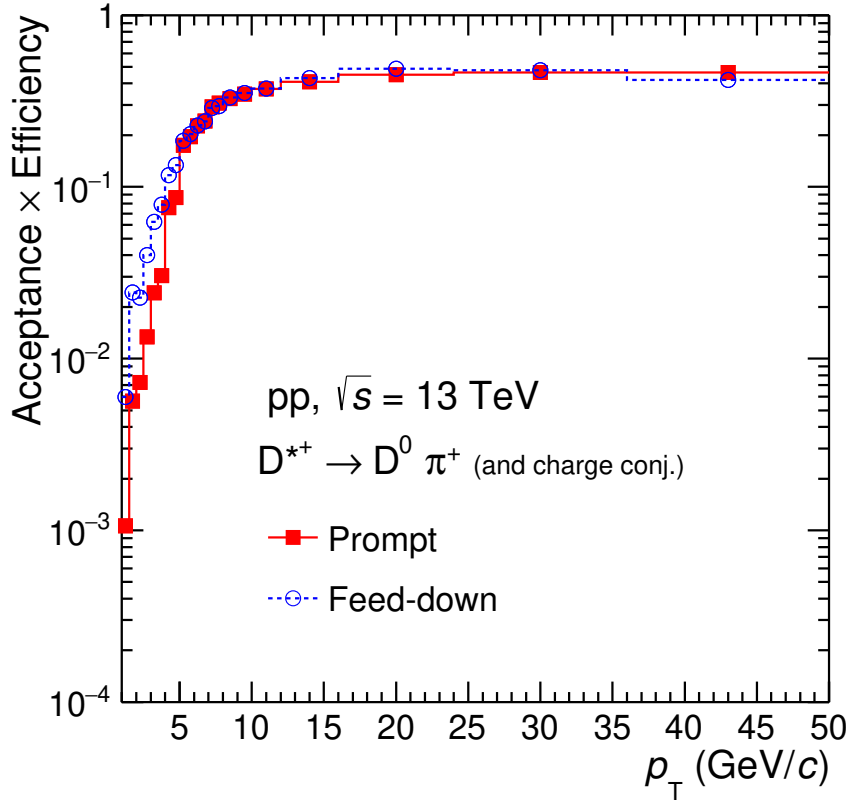


Fig. 5: Transverse momentum dependence of Acceptance×Efficiency for prompt and feed-down.

4 Systematic uncertainties

4.1 Raw yield extraction

Several sources of systematic errors were considered for the D^{*+}-meson analysis. The systematic error on the yield extraction was determined by repeating the fitting procedure described in section 2.4 with a different mass range, different histogram bin widths and/or different fitting functions, and using a method based on bin counting after the subtraction of the background estimated from the fit of the side bands.

The systematic uncertainty on the raw yield extraction was evaluated in each p_T interval using a multiple trial approach. The fits to the invariant mass distributions were repeated several times varying:

- i) the invariant-mass bin width (six different bin widths);
- ii) lower limit of the fit (0.1395, 0.140, 0.1405);
- iii) upper limit of the fit (0.165, 0.163, 0.161, 0.159, 0.157, 0.155);
- iv) the background fit function (2 cases: PowerLaw $a(x - m_\pi)^b$, PowerLaw \times Exponential (Eq. 1));

In addition bin counting at 3σ was tested, and fixing the Gaussian sigma to the one extracted from the MC simulation and the mean of the Gaussian function to the PDG value of the D^{*+} mass. The fits which did not converge or had $\chi^2/ndf > 3.0$ were rejected and not considered in the evaluation of the systematic uncertainty. In addition, the results obtained with the fitting technique were compared to those obtained by counting the entries in the invariant mass histogram after subtracting the background counts calculated from the background fit function. Also for this check, a multiple trial approach was used. The results of the multiple trial approach are shown in figure 10, 11, 12, 13, and 14.

For the first two p_T bins, some checks were performed to investigate the background fit function used in the trial, power law and power law \times exponential function. All the checks can be seen in figures 6, 7, 8, 9, and 15. For p_T bin 1-1.5 GeV/ c , the power law and power law \times exponential background function doesn't describe well the invariant mass distribution. For p_T bin 1.5-2 GeV/ c , the power law function leads to significantly larger widths. The numerical values of the systematic on yield extraction are reported in Tables 3.

p_T (GeV/ c)	1-1.5	1.5-2	2-2.5	2.5-3	3-3.5	3.5-4	4-4.5	4.5-5	5-5.5	5.5-6	6-6.5
Systematic values	10%	10%	5%	2%	2%	2%	2%	2%	2%	2%	2%

p_T (GeV/ c)	6.5-7	7-7.5	7.5-8	8-9	9-10	10-12	12-16	16-24	24-36	36-50
Systematic values	2%	2%	2%	2%	2%	2%	2%	2%	2%	2%

Table 3: Systematic uncertainty from yield extraction.

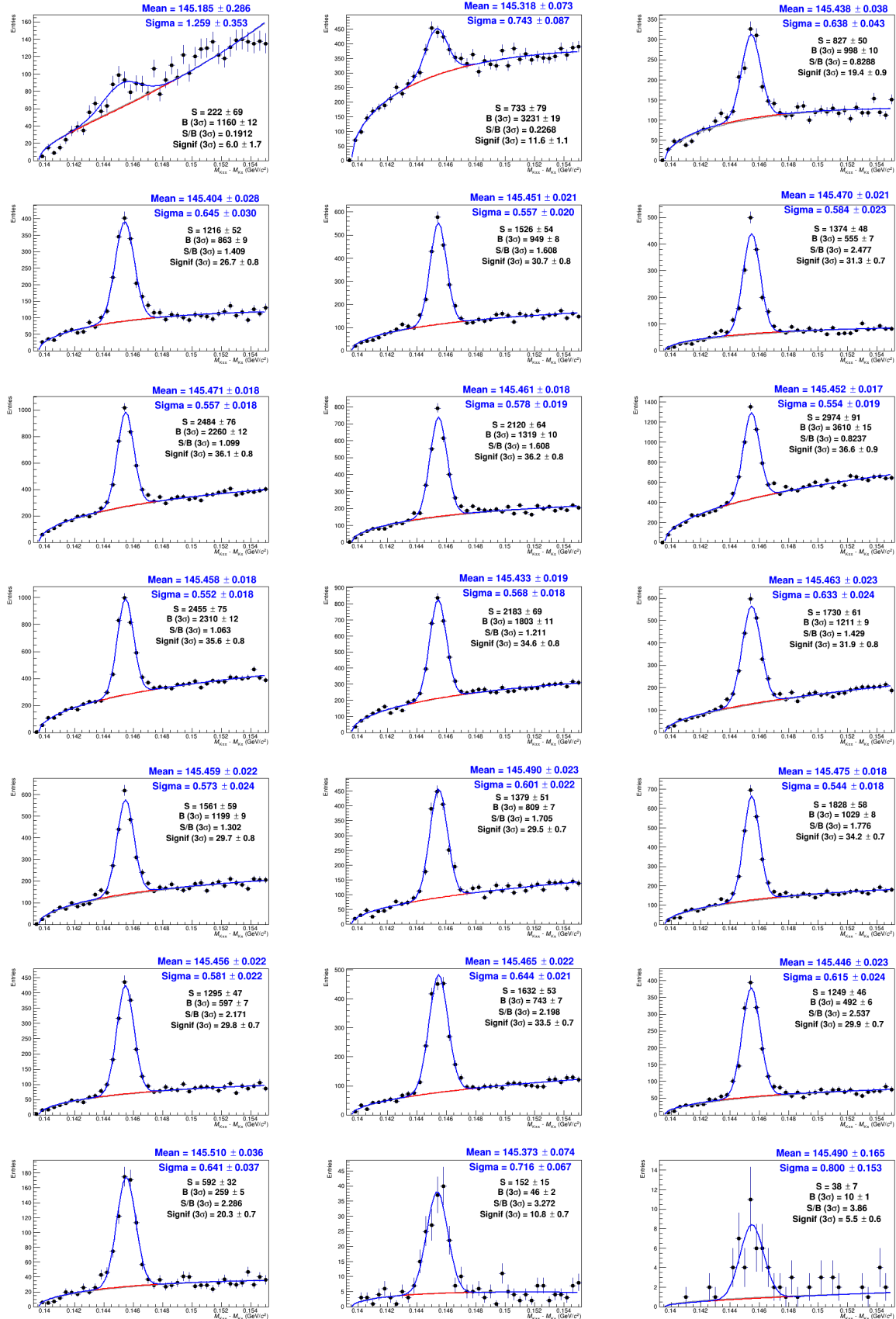


Fig. 6: D⁺ signal extraction using standard background fit function, power law × exponential.

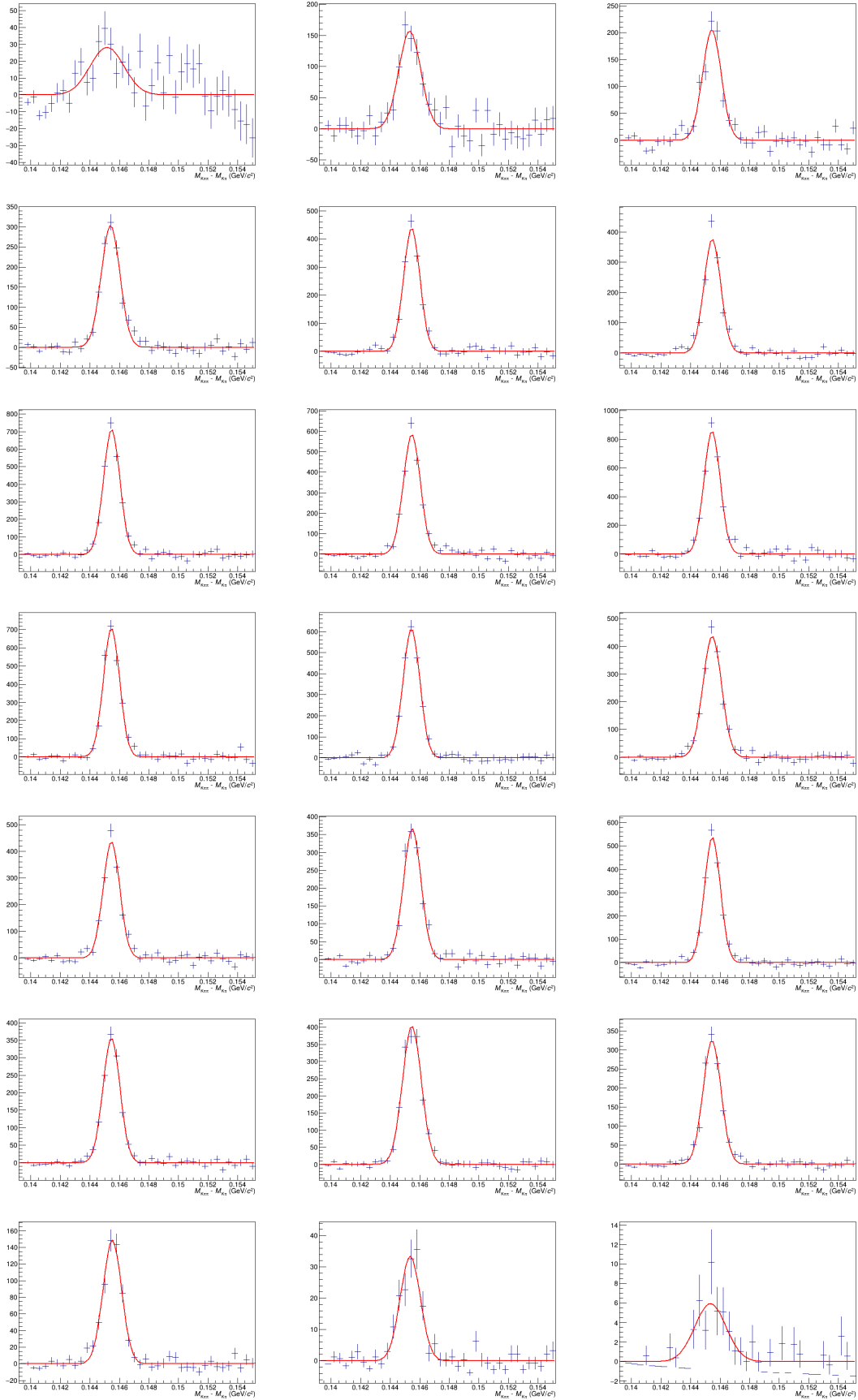


Fig. 7: Residual plots using standard background fit function.

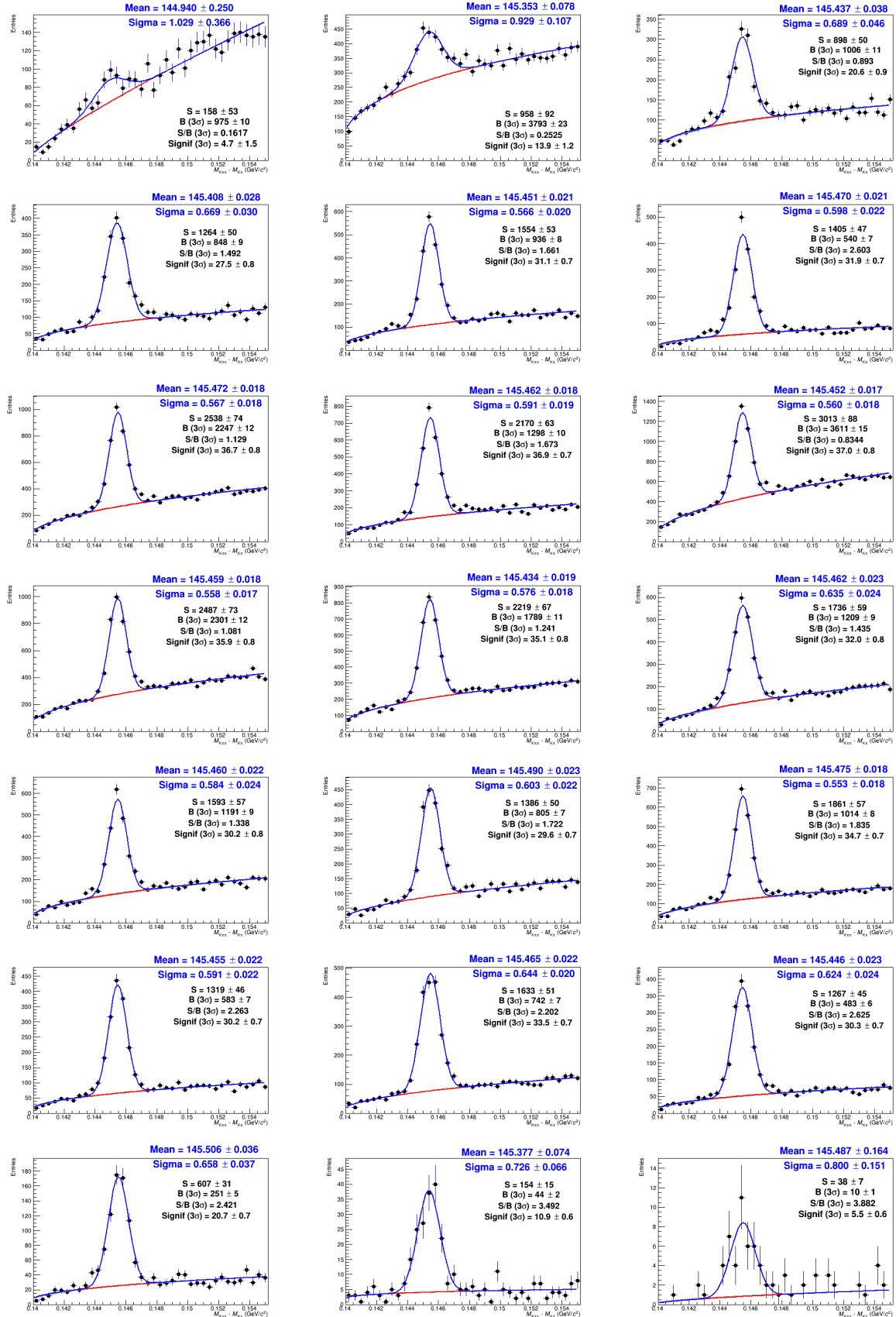


Fig. 8: D^{*+} signal extraction using a power fit function for background.

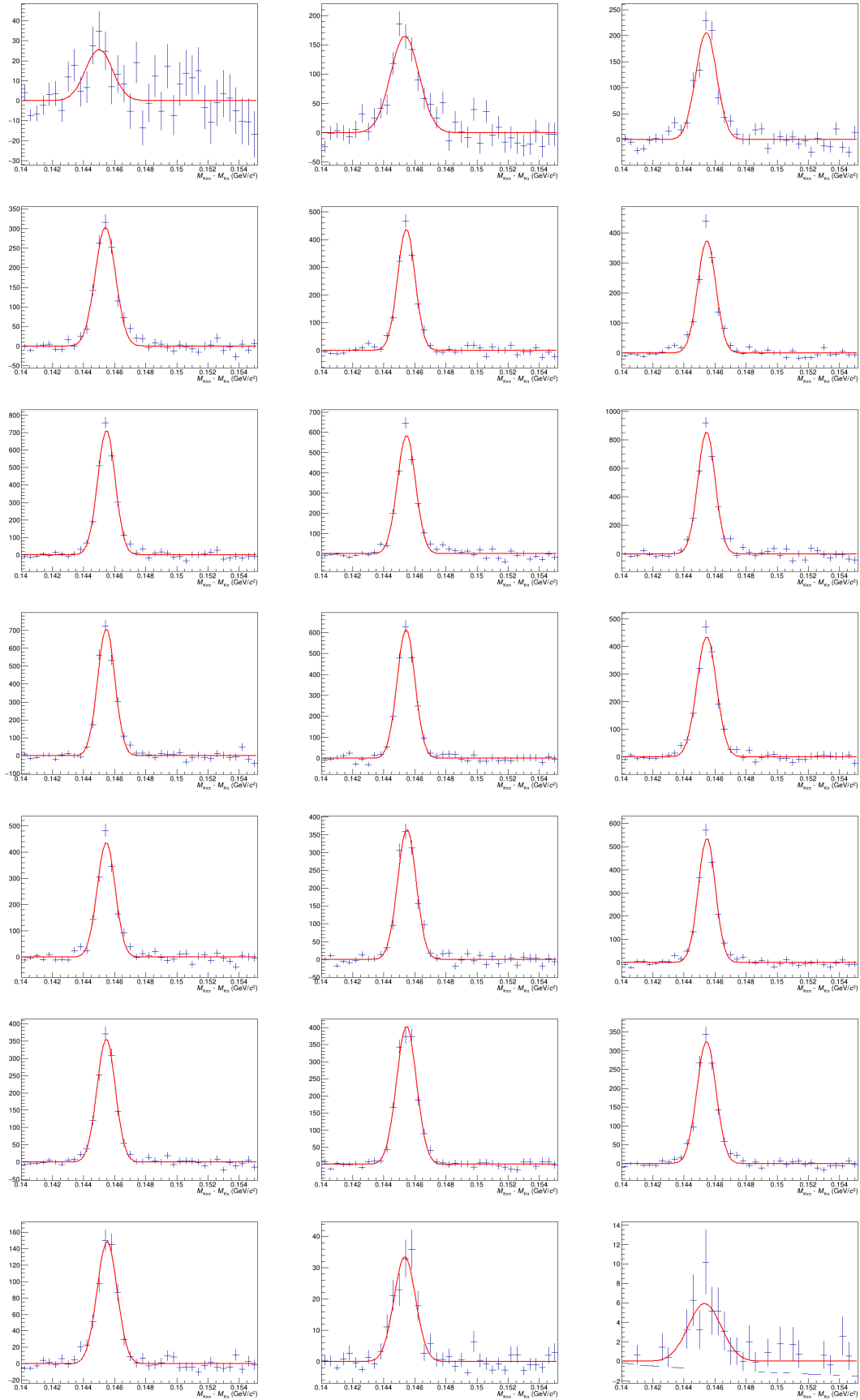


Fig. 9: Residual plots using power fit function for background shape.

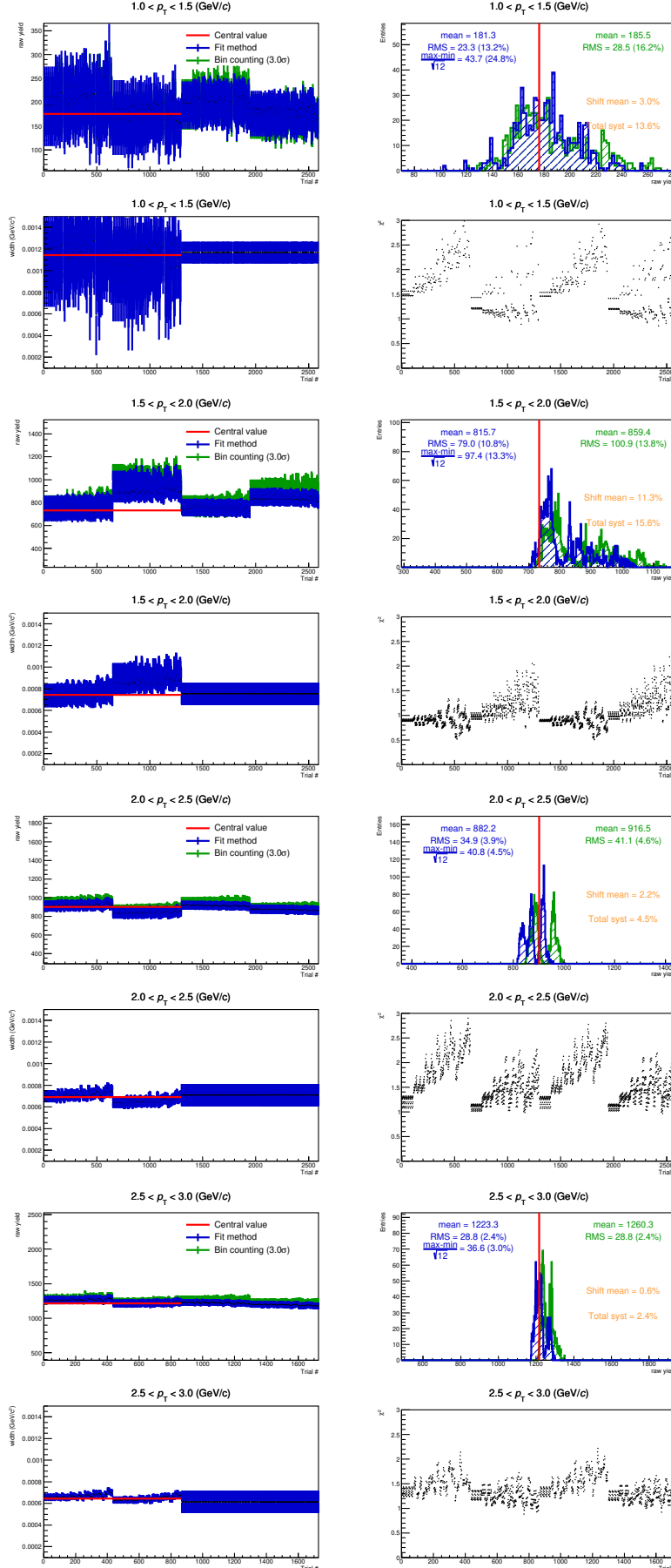


Fig. 10: Output of the multi-trial study for D^{*+} mesons for $1 < p_T < 3 \text{ GeV}/c$. For each p_T bin: the top panel shows the raw yield as a function of trials and raw yield distributions, the bottom panel shows the width and χ^2 as a function of trials.

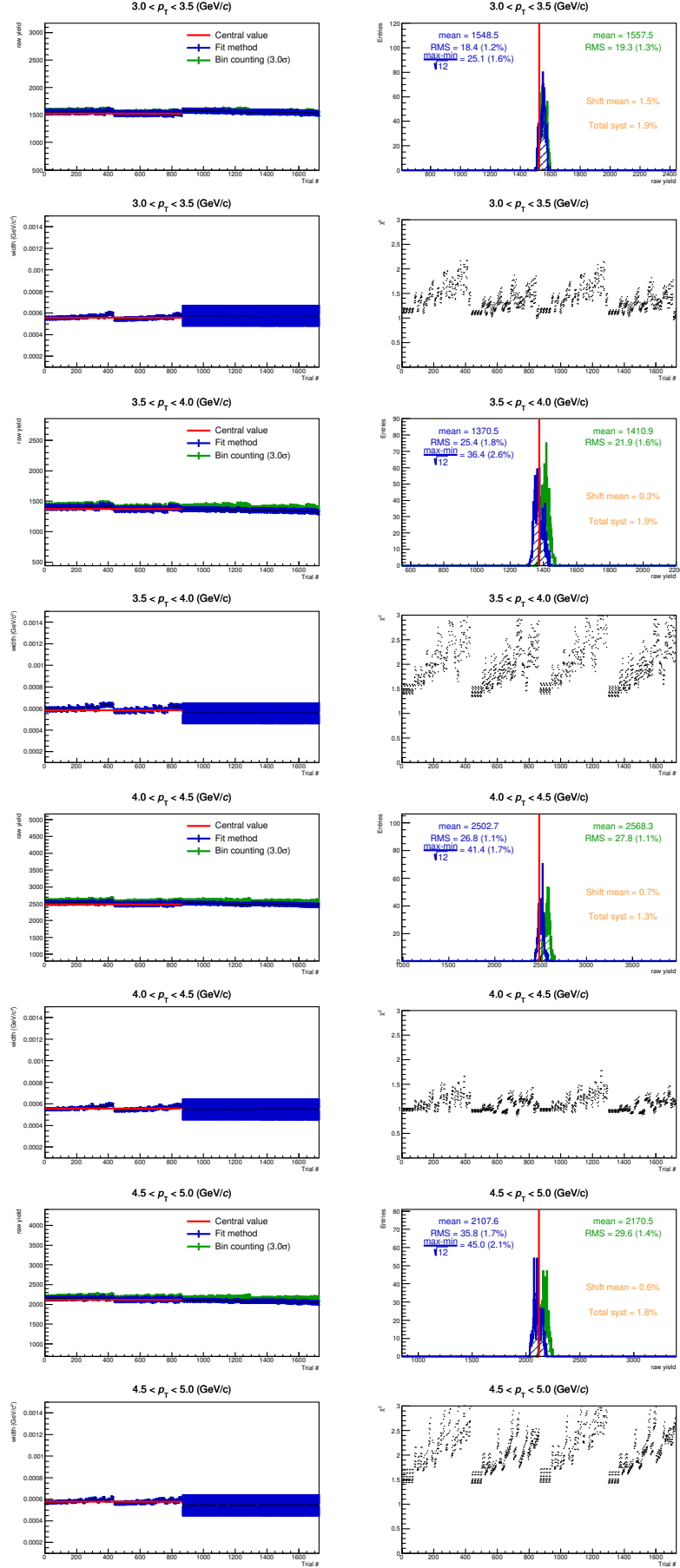


Fig. 11: Output of the multi-trial study for D^{*+} mesons for $3 < p_T < 5$ GeV/c. For each p_T bin: the top panel shows the raw yield as a function of trials and raw yield distributions, the bottom panel shows the width and χ^2 as a function of trials.

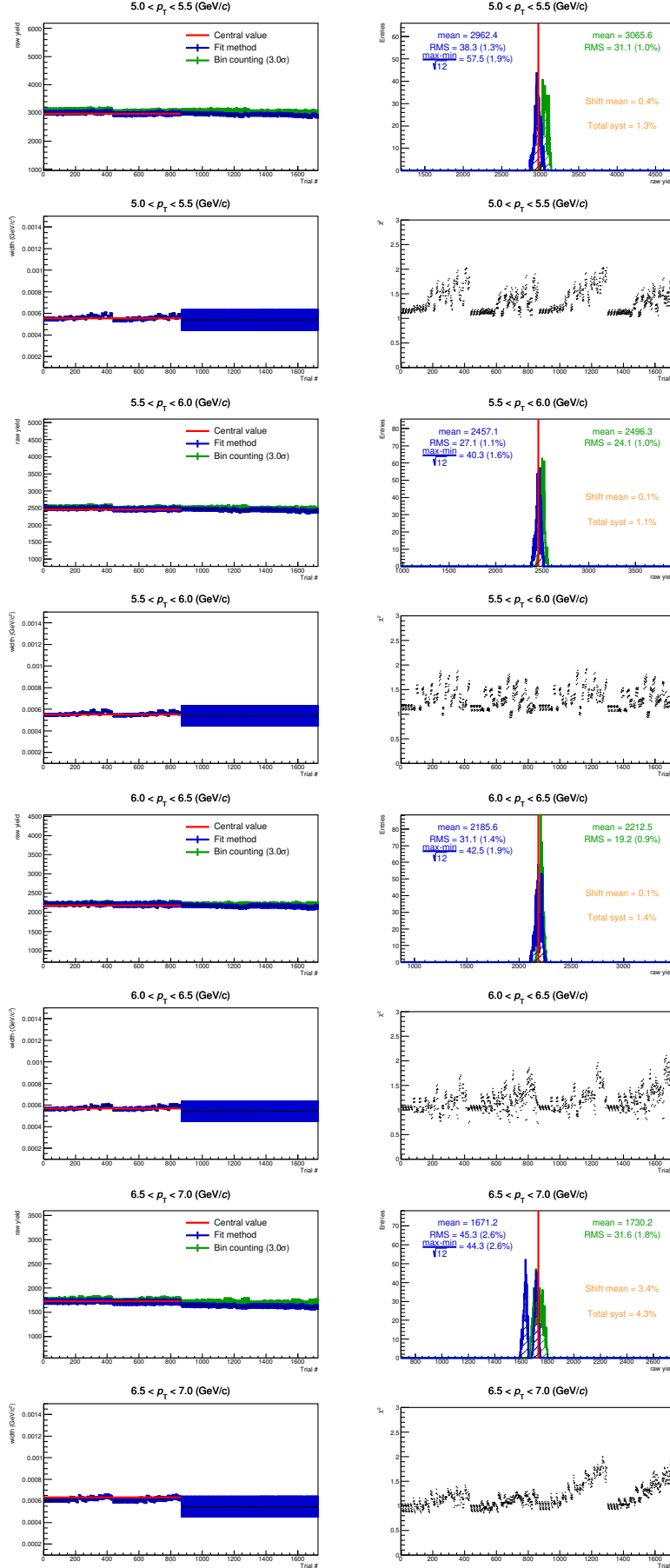


Fig. 12: Output of the multi-trial study for D^{*+} mesons for $5 < p_T < 7 \text{ GeV}/c$. For each p_T bin: the top panel shows the raw yield as a function of trials and raw yield distributions, the bottom panel shows the width and χ^2 as a function of trials.

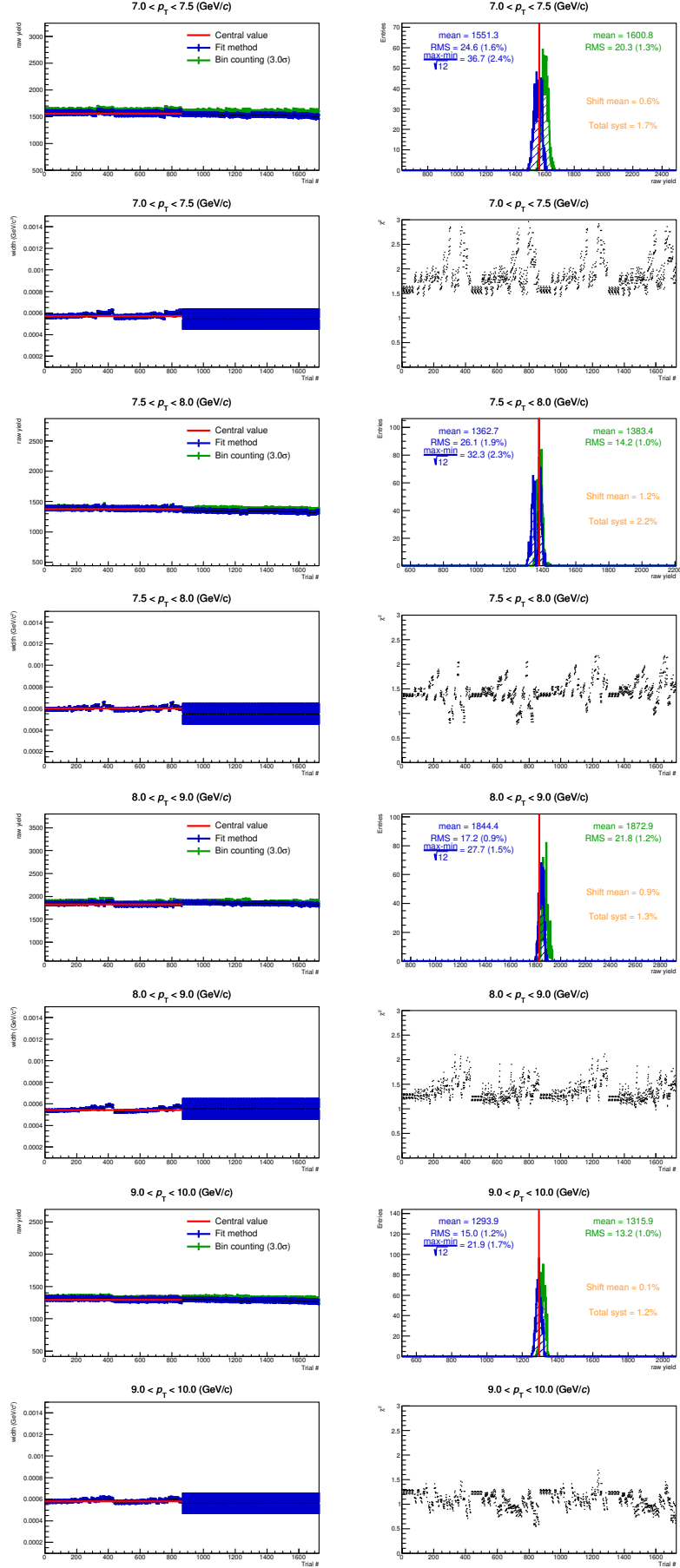


Fig. 13: Output of the multi-trial study for D^{*+} mesons for $7 < p_T < 10$ GeV/c. For each p_T bin: the top panel shows the raw yield as a function of trials and raw yield distributions, the bottom panel shows the width and χ^2 as a function of trials.

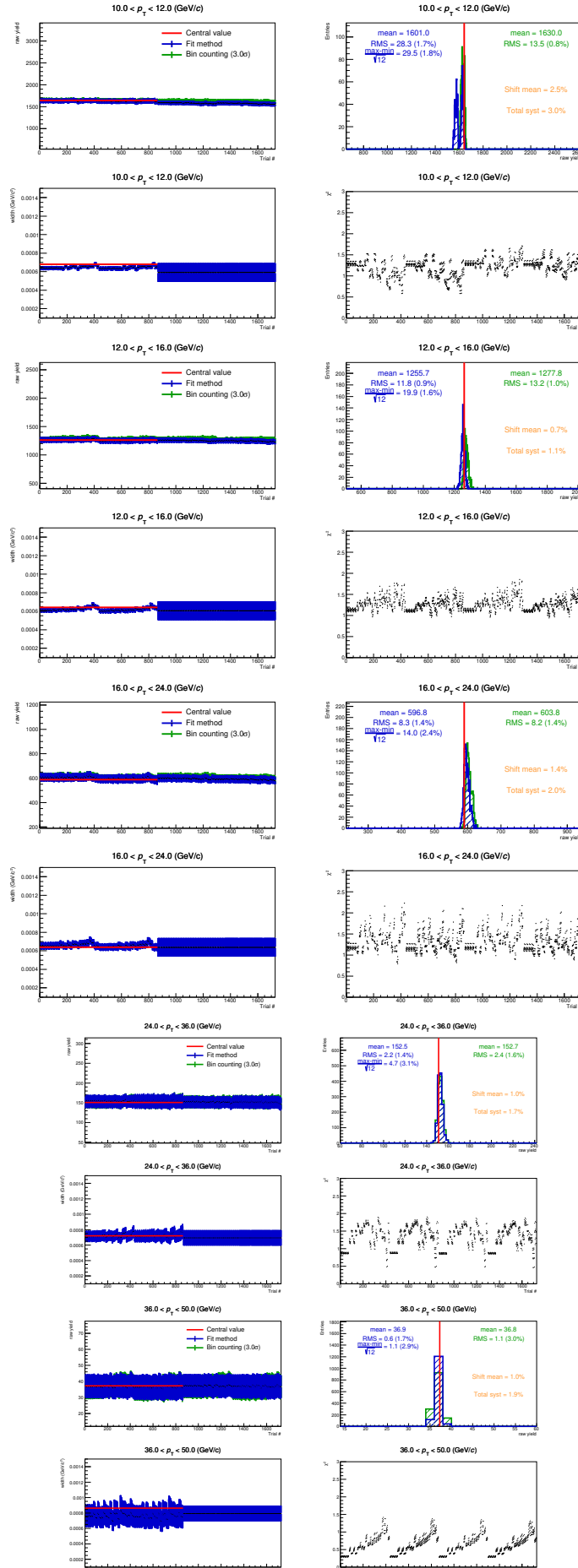


Fig. 14: Output of the multi-trial study for D^{*+} mesons for $10 < p_T < 50$ GeV/c. For each p_T bin: the top panel shows the raw yield as a function of trials and raw yield distributions, the bottom panel shows the width and χ^2 as a function of trials.

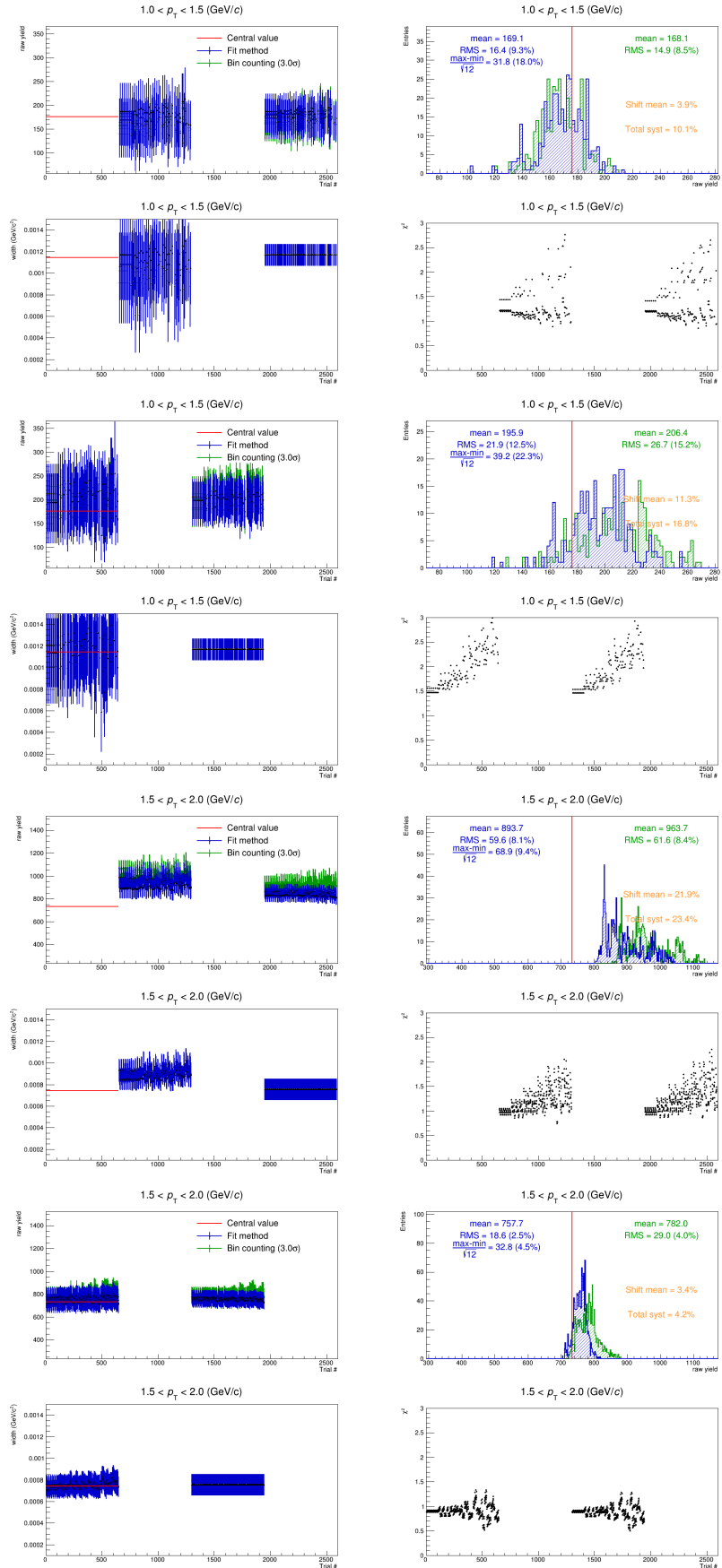


Fig. 15: Yield extraction for transverse momentum range $1 < p_T < 2$ GeV/c tested with only one background function for each p_T bin, 1-1.5 GeV/c and 1.5-2 GeV/c.

4.2 Selection efficiency

The systematic uncertainty due to possible imperfections in the description in the simulations of the variables used in the geometrical selections of the D^{*+} -meson displaced decay vertices was studied by repeating the analysis varying the applied selection criteria.

The systematic scan for D^{*+} -meson from loose to tight cuts was done by varying the variables: DCA, d_0 pion and d_0 kaon, $d_0^K \times d_0^\pi$, cosine θ point, and normalised decay length. The result of this study is shown in figure 16, where the variation of the rawyield, prompt efficiency, and corrected yield ratio are plotted as a function of the cut set tested. The systematic values are reported in Table 4.

p_T (GeV/c)	Systematic values
1.0-1.5	10%
1.5-2.0	6%
2.0-2.5	6%
2.5-3.0	4%
3.0-3.5	4%
3.5-4.0	2%
4.0-4.5	2%
4.5-5.0	2%
5.0-5.5	2%
5.5-6.0	2%
6.0-6.5	2%
6.5-7.0	2%
7.0-7.5	2%
7.5-8.0	2%
8.0-9.0	2%
9.0-10.0	2%
10.0-12.0	2%
12.0-16.0	2%
16.0-24.0	2%
24.0-36.0	2%
36.0-50.0	2%

Table 4: Systematic uncertainty estimated with the cut-variation study.

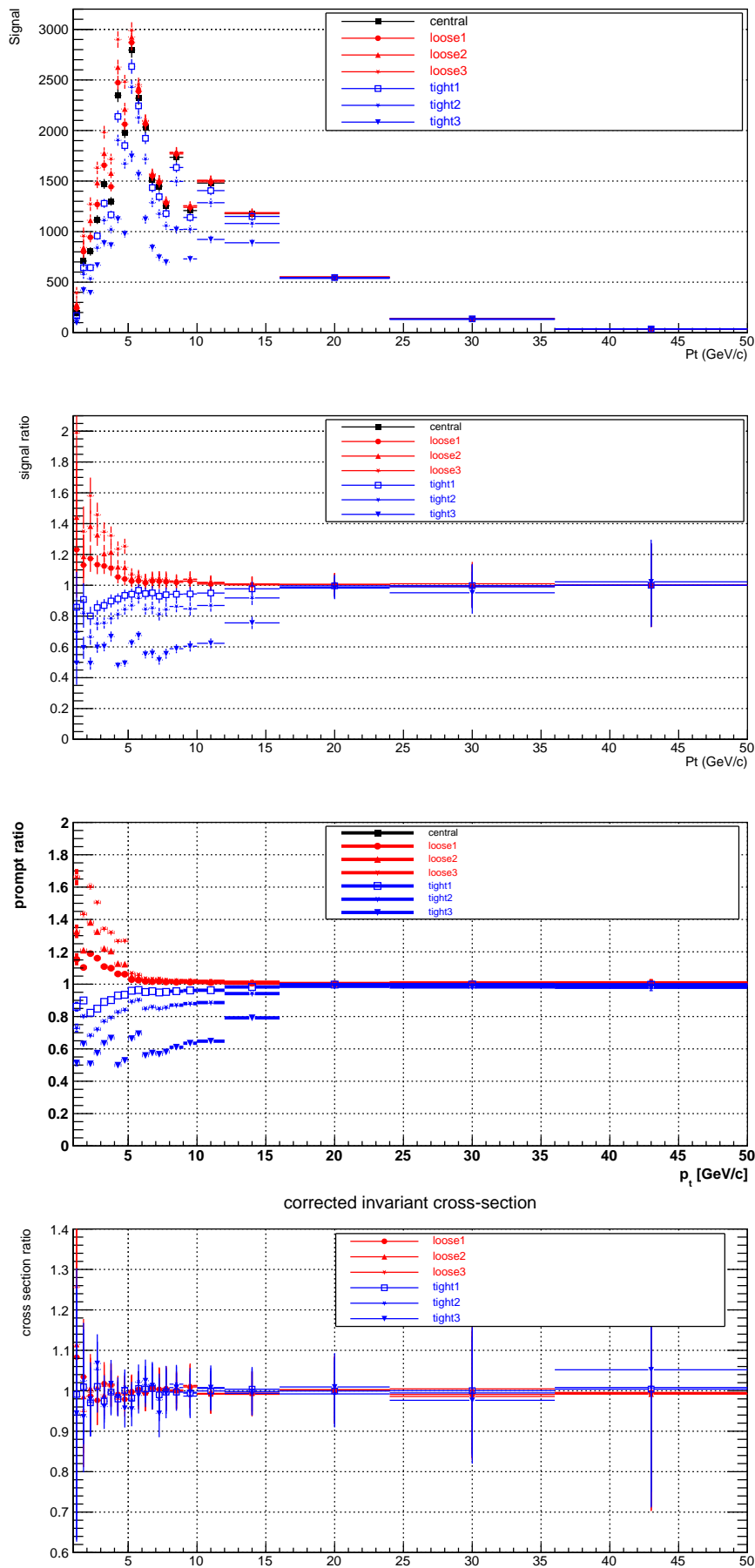


Fig. 16: Variations of raw yield (the first two figures from top), prompt efficiency, and corrected yield (bottom) obtained with the cut-variation.

4.3 Generated p_T shape

Another source of systematic we investigated is the one arising from the D meson p_T shape assumed in the Monte Carlo used for corrections. In our simulation the D mesons are folded in the HIJING event using PYTHIA and as a result the p_T shape of the D mesons can be biased leading to an effect in the final efficiency used for corrections. In order to check the stability of our efficiencies against the change in p_T shape and to define a systematic uncertainty it was decided to implement several set of weights.

The systematic uncertainty due to a possible difference between the real and simulated D-meson transverse momentum distributions was investigated. The uncertainty was estimated by weighting the assumed PYTHIA8 D^{*+} p_T distribution in simulation with alternative p_T shapes. The systematic uncertainty was evaluated comparing the central values of the efficiency obtained using the FONLL p_T weight. The p_T shapes and the corresponding p_T weights, obtained by dividing each shape by the one of the MC simulation, are reported in figure 17 and 18. A 3% systematic was assigned in the range $1 < p_T < 1.5 \text{ GeV}/c$, 0.5% in the range $1.5 < p_T < 2 \text{ GeV}/c$ while no systematic uncertainty was assigned for $p_T > 2 \text{ GeV}/c$.

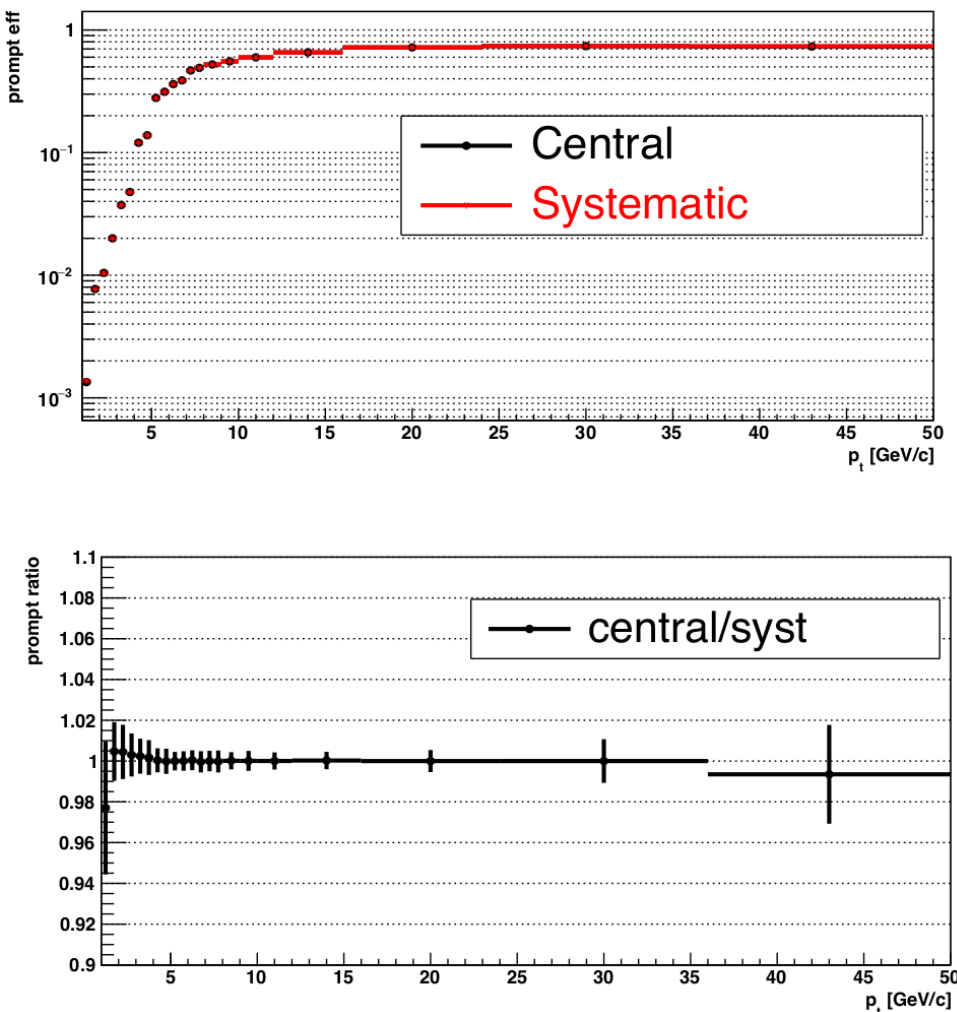


Fig. 17: Relative change in efficiencies by using PYTHIA8 (central) with respect to FONLL (systematic) weight.

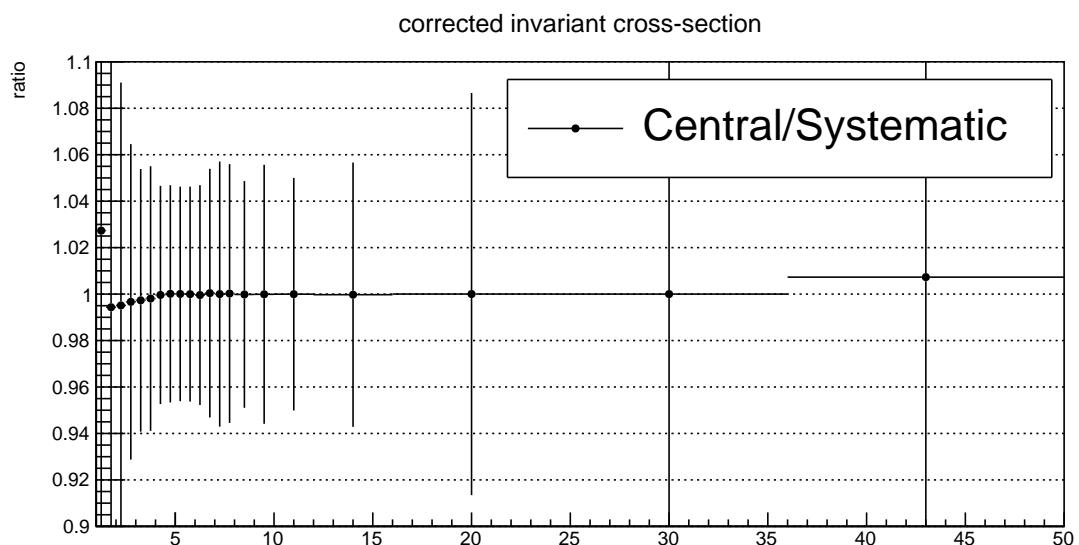


Fig. 18: Relative change in efficiencies by using PYTHIA8 (central) with respect to FONLL (systematic) weight.

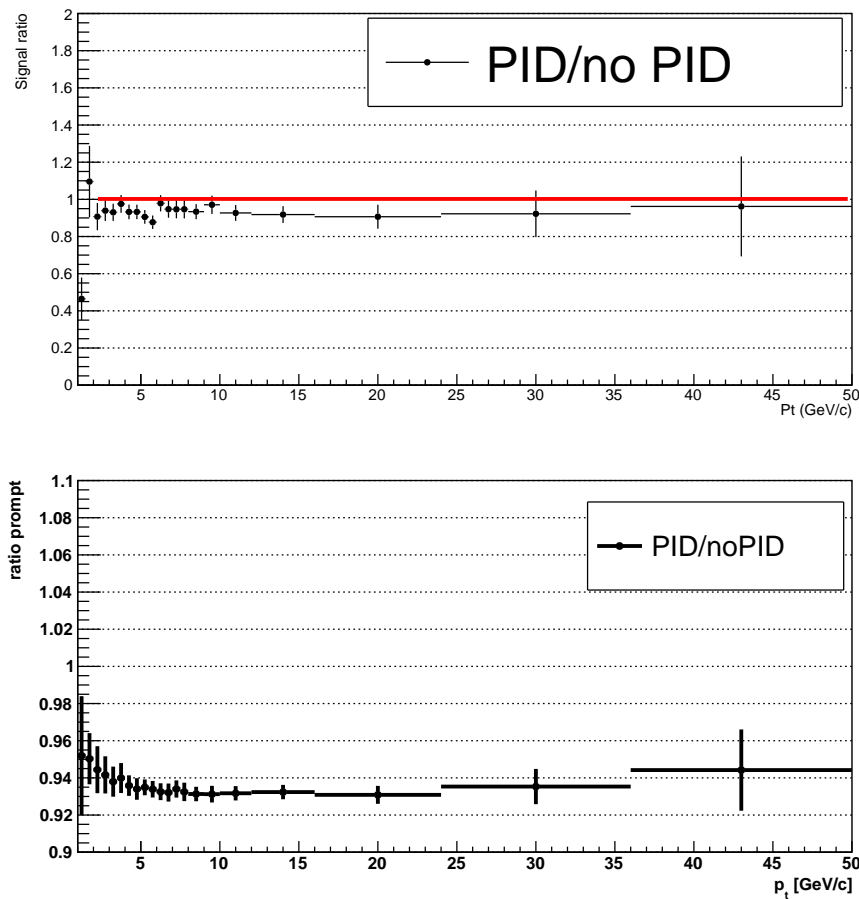


Fig. 19: Ratio of raw yield (top) and prompt efficiency (bottom) obtained with and without PID.

4.4 PID efficiency

The systematic effect due to the particle identification (PID) selections was studied by repeating the analysis without PID selection. The uncertainty was evaluated by comparing the corrected yield ratio obtained with and without PID, which is shown in figure 19 and 20. All the points are compatible with unity, most of them at better than 1σ level. Therefore, no systematic uncertainty was assigned to PID efficiency.

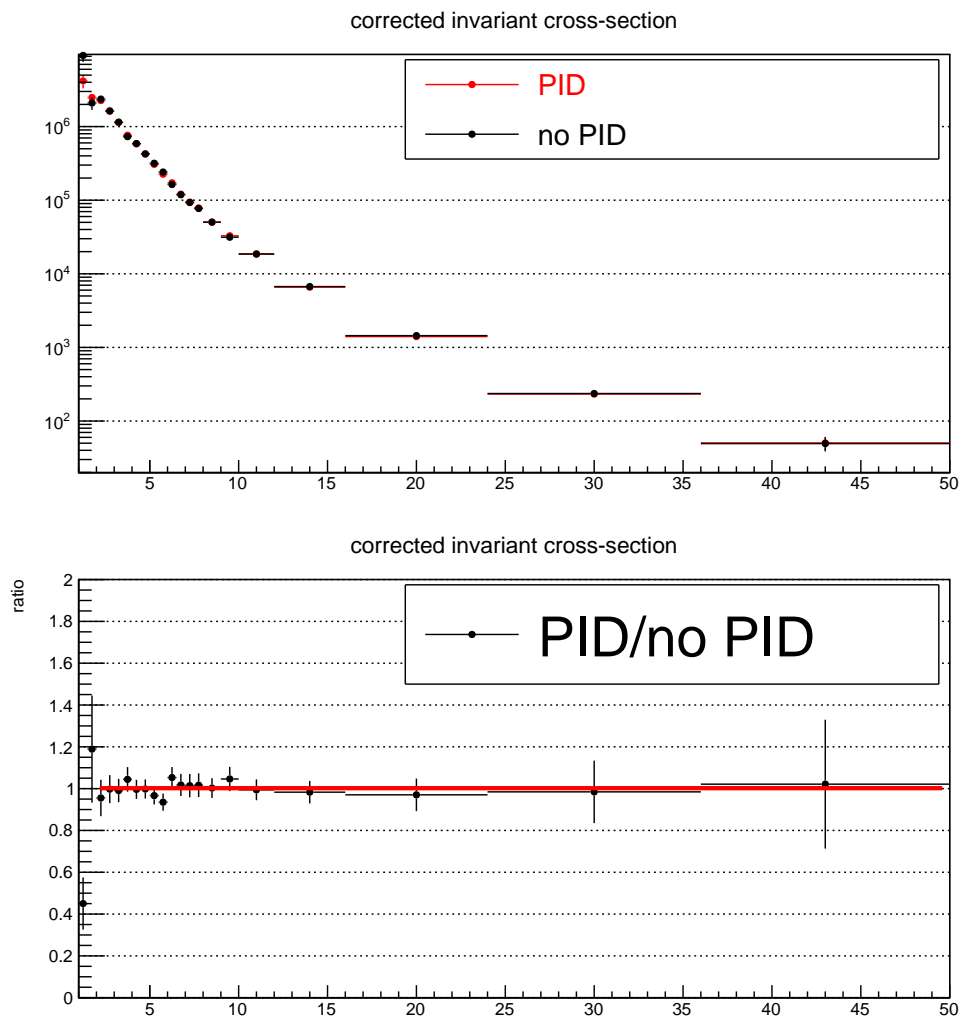


Fig. 20: Comparison of D^{*+} cross sections obtained with and without PID.

4.5 Track reconstruction efficiency

The systematic uncertainty due to the track-reconstruction efficiency includes the contributions of the track-finding procedure in the TPC detector and prolongation in the ITS detector, and the track-quality selections.

The ITS-TPC matching efficiency was computed as the number of tracks successfully fitted with the Kalman filter in the TPC and ITS, with at least one hit in the SPD layers, divided by the number of reconstructed tracks successfully fitted in the TPC. The systematic uncertainty on its determination arises from discrepancies in the tracking performance between data and the MC simulation. The ITS-TPC matching efficiency is different for particles produced in the collision, including strong decays and weak decays of charm and beauty hadrons, which are considered as primary particles in this study, and secondary particles (i.e. particles produced in the interactions with the material or in decays of strange hadrons). The HIJING event generator and the GEANT3 transport package do not reproduce the relative abundance of primary and secondary particles, therefore data-driven corrections for the fraction of primary particles (f_{primary}) were used to weight the MC simulation and obtain the corrected inclusive MC efficiency ($\epsilon_{\text{inclusive}}(\text{MC})$), which is computed as:

$$\epsilon_{\text{inclusive}}(\text{MC}) = f_{\text{primary}} \cdot \epsilon_{\text{primary}}(\text{MC}) + (1 - f_{\text{primary}}) \cdot \epsilon_{\text{secondary}}(\text{MC}), \quad (3)$$

where $\epsilon_{\text{primary}}(\text{MC})$ and $\epsilon_{\text{secondary}}(\text{MC})$ are the ITS-TPC matching efficiencies for primary and secondary particles, which are determined via fits to the d_0^{xy} distributions of the tracks.

In addition, it was checked if a discrepancy between the efficiency of the track-quality selections in data and in the MC simulation need to be considered. For this purpose, the D-meson cross section was re-evaluated with three alternative track-quality selection criteria, which include the selection of tracks with (i) a number TPC crossed rows larger than $120 - 5/(p_T [\text{GeV}/c])$, (ii) the number of TPC clusters at least 0.65 times the number of TPC crossed rows and (iii) a ratio of crossed rows over findable clusters in the TPC larger than 0.9 (being the default 0.8). These variations are shown in figure 21. The variation of the cross section was observed to be around 1.0% for D^0 (two-body decay) and 2% for the soft pion track. The systematic uncertainties are shown in figure 22. The systematic values are reported in Table 5.

$p_T (\text{GeV}/c)$	1-1.5	1.5-2	2-2.5	2.5-3	3-3.5	3.5-4	4-4.5	4.5-5	5-5.5	5.5-6	6-6.5
Systematic values	4.5%	4.5%	5%	5%	5%	5%	5.5%	5.5%	5.5%	5.5%	5.5%

$p_T (\text{GeV}/c)$	6.5-7	7-7.5	7.5-8	8-9	9-10	10-12	12-16	16-24	24-36	36-50
Systematic values	6%	6%	6%	6%	6%	6%	6%	6.5%	6.5%	6.5%

Table 5: Systematic uncertainty from tracking efficiency.

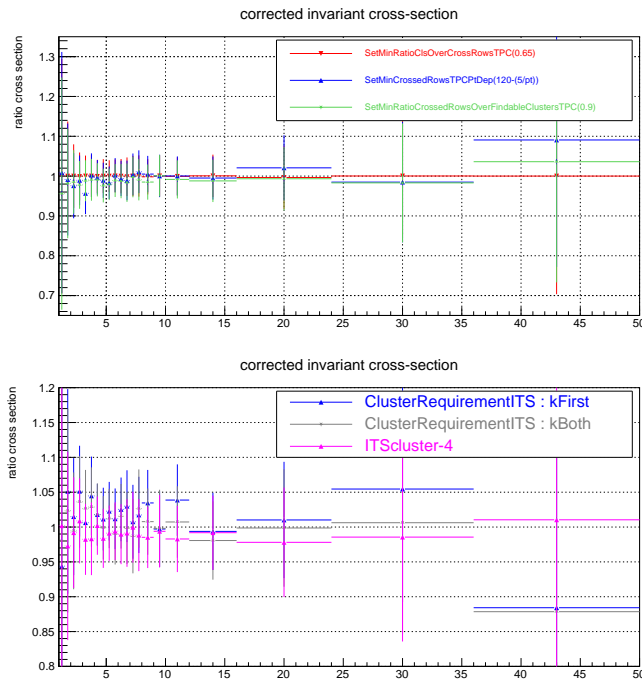


Fig. 21: Comparison of D^{*+} corrected yield measured obtained with different TPC track-quality criteria.

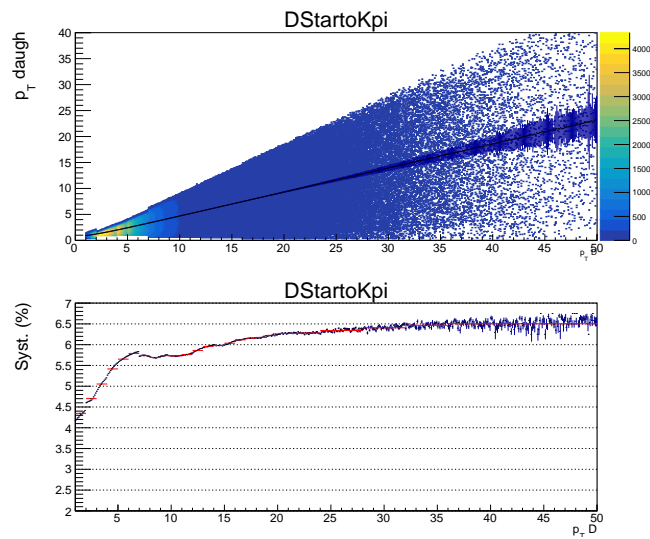


Fig. 22: Top: scatter plot of daughter p_T versus D^{*+}-meson p_T . Bottom: final systematic uncertainties propagated at D^{*+}-meson level after weighting for daughter's kinematics.

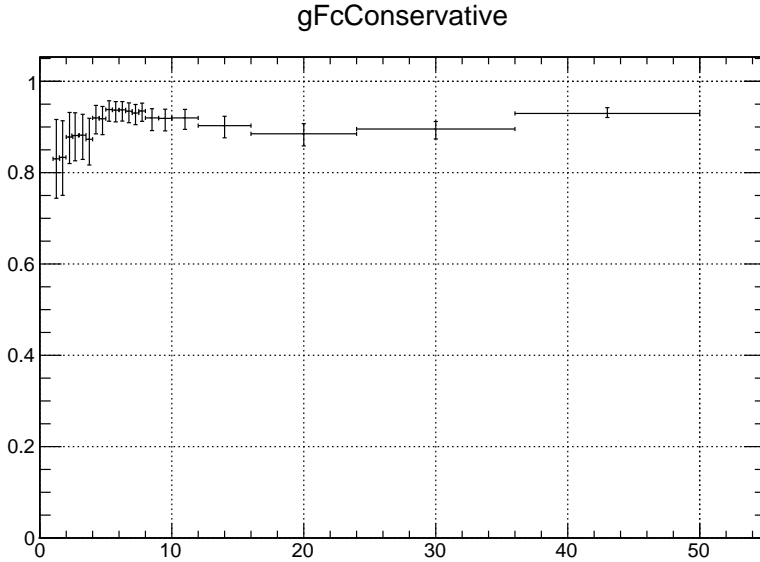


Fig. 23: Fraction of prompt D^{*+} estimated using the FONLL-based approach.

5 Feed-down subtraction

The feed-down contribution was estimated using the beauty production cross section from the FONLL calculation, the $B \rightarrow D$ decay kinematics from the EvtGen package, and the Monte Carlo efficiencies for feed-down D mesons. Thus, omitting for brevity the symbol of the p_T -dependence (p_T), the fraction of prompt D mesons reads:

$$\begin{aligned} f_{\text{prompt}} &= 1 - (N^D \text{ feed-down raw} / N^D \text{ raw}) \\ &= 1 - \left(\frac{d^2\sigma}{dy dp_T} \right)_{\text{feed-down}}^{\text{FONLL}} \cdot \frac{(Acc \times \epsilon)_{\text{feed-down}} \cdot \Delta y \Delta p_T \cdot BR \cdot L_{\text{int}}}{N^D \text{ raw} / 2}, \end{aligned} \quad (4)$$

where $(Acc \times \epsilon)_{\text{feed-down}}$ is the acceptance-times-efficiency for feed-down D mesons and the factor 2 at the denominator comes for counting both particle and antiparticle are combined while in FONLL not.

The systematic uncertainties on the prompt fraction of D^{*+} -meson f_{prompt} , estimated via the Nb method is performed by varying the parameters used in the FONLL B predictions, are shown in figure 23.

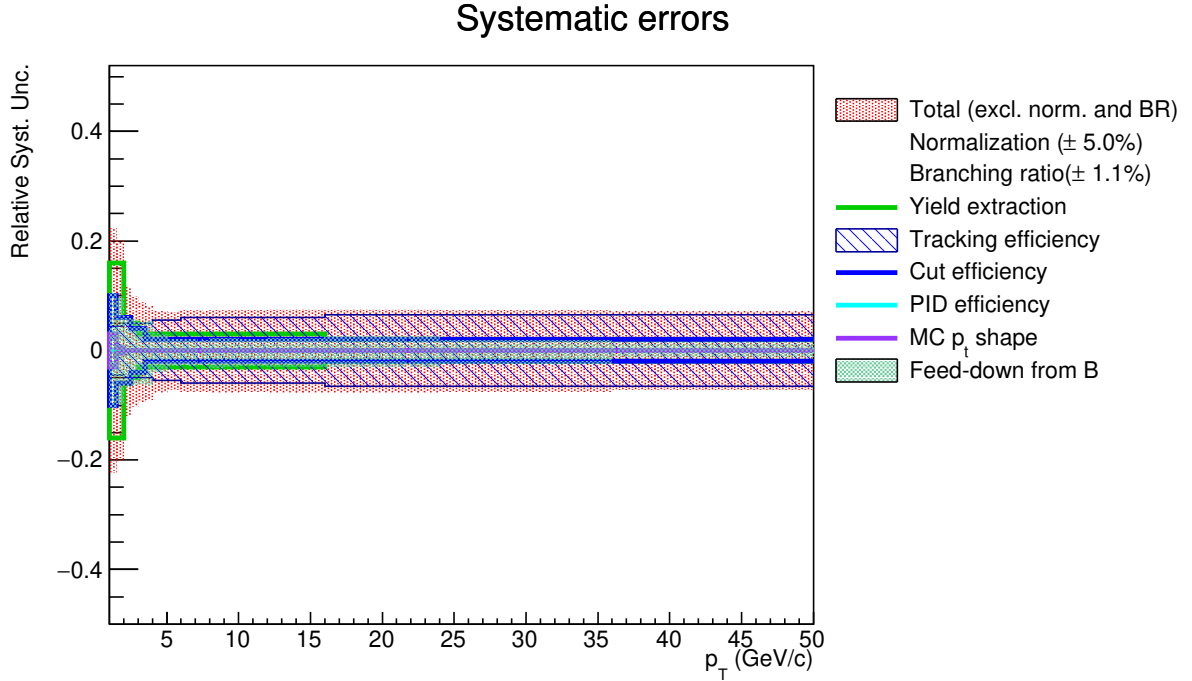


Fig. 24: Relative systematic uncertainties on the p_T -differential production cross section of prompt D^{*+}.

6 D^{*+}-meson systematics summary

The summary for all systematics is shown in figure 24. The systematic uncertainties for this analysis are reported in Table 6.

p_T (GeV/c)	1-1.5	1.5-2	2-2.5	2.5-3	3-3.5	3.5-4	4-4.5	4.5-5	5-5.5	5.5-6	6-6.5
Raw yield	10%	10%	5%	2%	2%	2%	2%	2%	2%	2%	2%
Cut variations	10%	6%	6%	4%	4%	2%	2%	2%	2%	2%	2%
MC p_T -shape	3%	0.5%	0%	0%	0%	0%	0%	0%	0%	0%	0%
PID	0%	0%	0%	0%	0%	0%	0%	0%	0%	0%	0%
Tracking	4.5%	4.5%	5%	5%	5%	5%	5.5%	5.5%	5.5%	5.5%	5.5%

p_T (GeV/c)	6.5-7	7-7.5	7.5-8	8-9	9-10	10-12	12-16	16-24	24-36	36-50
Raw yield	2%	2%	2%	2%	2%	2%	2%	2%	2%	2%
Cut variations	2%	2%	2%	2%	2%	2%	2%	2%	2%	2%
MC p_T -shape	0%	0%	0%	0%	0%	0%	0%	0%	0%	0%
PID	0%	0%	0%	0%	0%	0%	0%	0%	0%	0%
Tracking	6%	6%	6%	6%	6%	6%	6%	6.5%	6.5%	6.5%

Table 6: D^{*+} systematic uncertainties summary.

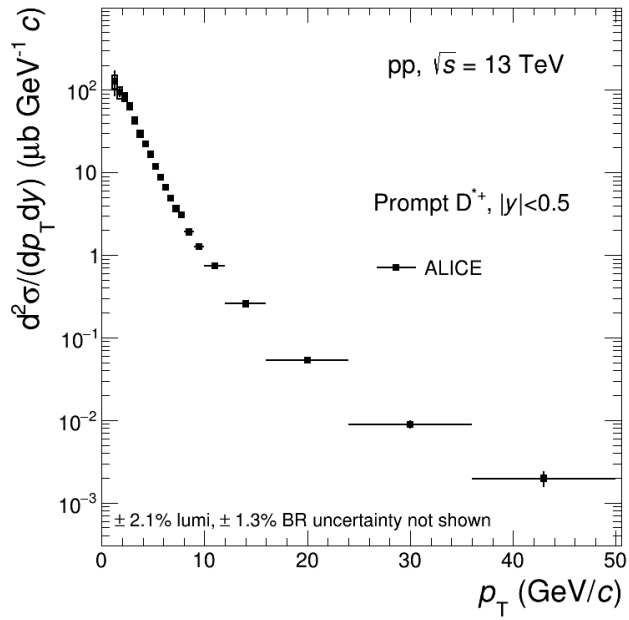


Fig. 25: p_T -differential inclusive production cross section of prompt D^{*+} mesons in pp collisions at $\sqrt{s} = 13$ TeV.

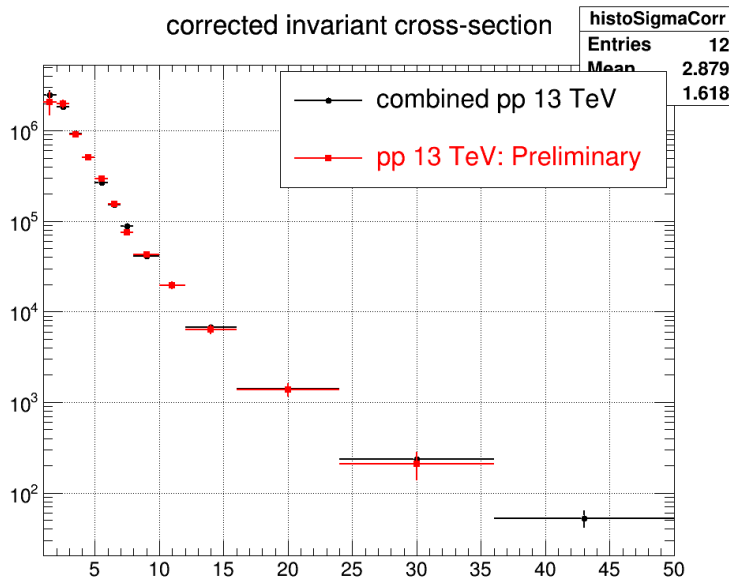


Fig. 26: Comparison new analysis full data sample (2016, 2017 and 2018) with respect to the only 2016 data in pp collisions at $\sqrt{s} = 13$ TeV.

7 Results

In this Section, the D^{*+} production cross sections are shown in Fig. 25. Figure 26 shows the comparison between the new analysis with full pp sample collected in 2016, 2017 and 2018 with respect to the old analysis only with data sample collected in 2016. The p_T -differential cross section of prompt D^{*+} is compared to theoretical model, FONLL, is shown in Fig. 27.

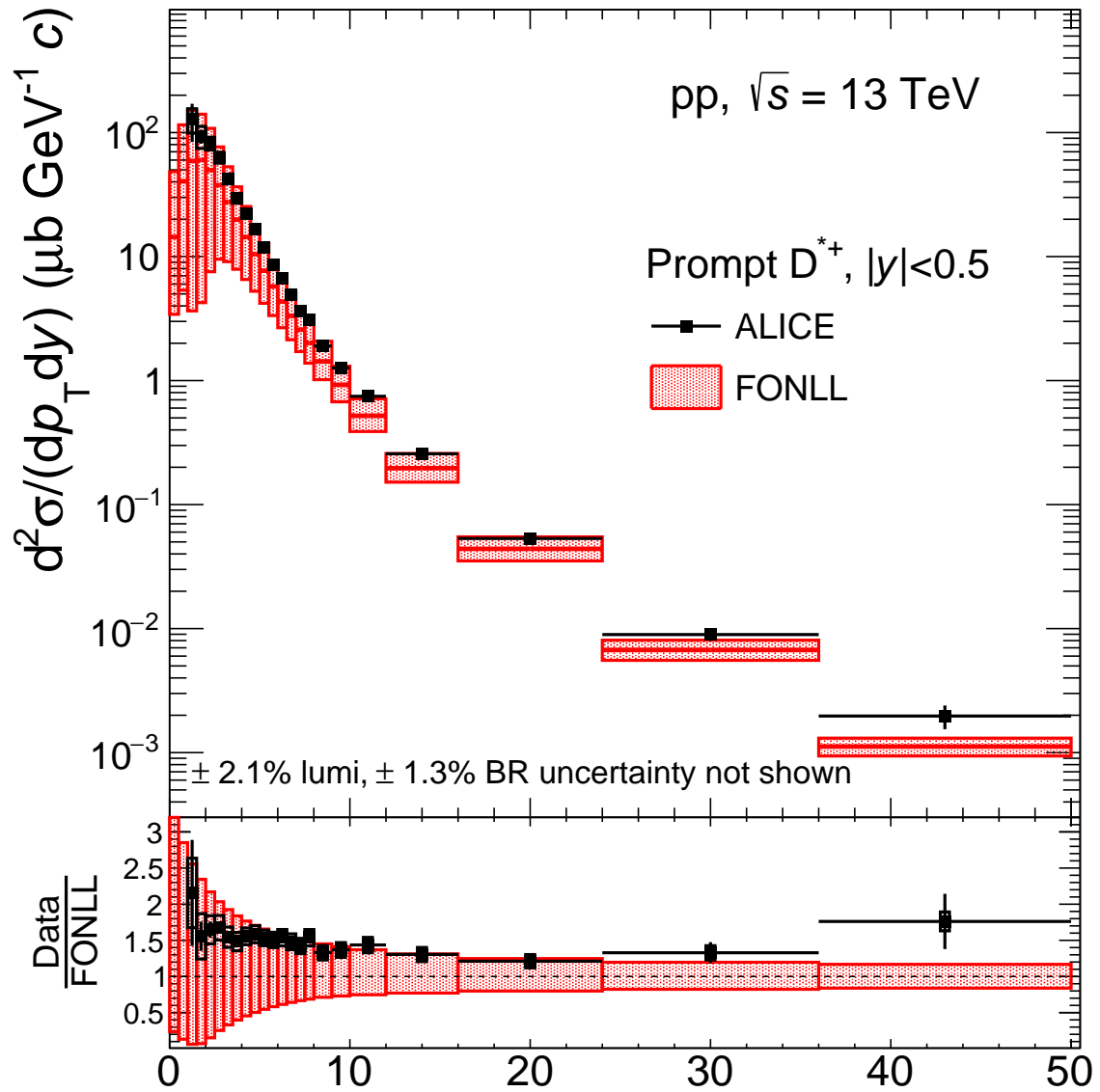


Fig. 27: p_T -differential inclusive production cross section of prompt D^{*+} mesons in pp collisions at $\sqrt{s} = 13$ TeV compared with FONLL.

References

- [1] ALICE Collaboration, J. Adam *et al.*, “Transverse momentum dependence of D-meson production in Pb-Pb collisions at $\sqrt{s_{\text{NN}}} = 2.76$ TeV,” *JHEP* **03** (2016) 081, arXiv:1509.06888 [nucl-ex].
- [2] ALICE Collaboration, “Analysis note,” <https://alice-notes.web.cern.ch/node/576>.
- [3] T. Sjostrand, S. Mrenna, and P. Skands, “PYTHIA 6.4 Physics and Manual,” *JHEP* **05** (2006) 026, arXiv:hep-ph/0603175 [hep-ph].
- [4] P. Z. Skands, “The Perugia Tunes,” in *Proceedings, 1st International Workshop on Multiple Partonic Interactions at the LHC (MPI08): Perugia, Italy, October 27-31, 2008*, pp. 284–297. 2009. arXiv:0905.3418 [hep-ph].
- [5] X.-N. Wang and M. Gyulassy, “HIJING: A Monte Carlo model for multiple jet production in p p, p A and A A collisions,” *Phys. Rev.* **D44** (1991) 3501–3516.
- [6] ALICE Collaboration, S. Acharya *et al.*, “Measurement of D^0 , D^+ , D^{*+} and D_s^+ production in pp collisions at $\sqrt{s} = 5.02$ TeV with ALICE,” arXiv:1901.07979 [nucl-ex].